Applied Acoustics 101 (2016) 201–221

Contents lists available at ScienceDirect

Applied Acoustics

journal homepage: www.elsevier.com/locate/apacoust

Modelling of the sound field radiated by multibeam echosounders for acoustical impact assessment

Xavier Lurton

Service Acoustique Sous-marine, Institut Français de Recherche pour l'Exploitation de la Mer (IFREMER), CS 10070, 29280 Plouzané, France

ARTICLE INFO

Article history:
Received 9 February 2015
Received in revised form 9 July 2015
Accepted 22 July 2015

Keywords:
Multibeam echosounders
Marine mammals
Sonar impact assessment
Sound Pressure Level
Sound Exposure Level
Directivity pattern

ABSTRACT

Multi-Beam Echo-Sounders (MBES) designed for seafloor-mapping applications are today a major tool for ocean exploration and monitoring. Concerns have been raised about their impact towards marine life and especially marine mammals, although their inherent characteristics (high frequencies, short signals and narrow transmitting lobes) actually minimize this possibility. The present paper proposes an analysis of MBES radiation characteristics (pulse design, source level and radiation directivity pattern) accounting for the various geometries met today and expressed according to the metrics used for acoustical impact assessment (maximum Sound Pressure Level, and cumulative Sound Exposure Level). A detailed radiation model is proposed, including the transmission through directivity sidelobes, and applied to three typical MBES examples. A simplified radiation model is then defined, in order to extend it to the case of the cumulative insonification by a MBES moving along a survey line. An approximated analytical model is proposed for the accumulated intensity, showing good agreement with the complete simulation of insonification; it is applied to the worst-case configuration of a low-frequency (12 kHz) multi-sector system. The computation of ranges corresponding to impact thresholds accepted today shows that impacts in terms of injury are negligible for both SPL and SEL; however behavioural response impacts cannot be excluded, and should require specific experimentation.

1. Introduction

1.1. Context and rationale

Multi-Beam Echo-Sounders (MBES) have been used for almost 40 years for seafloor mapping in support of chart-making, naval activities, and geoscience. As the resolution and capabilities of these systems have improved along the years, the applications have expanded to environmental monitoring and fisheries, surveys for hydrocarbon exploration, offshore engineering, coastal management and underwater archaeology. Structurally [1], these systems transmit a short sound pulse inside a wide angular sector steered vertically and across the carrier platform's track (Fig. 1). In reception they process the seafloor echoes inside a high number of narrow beams, providing a high selectivity in the measurement of sounding values along a number of angular directions together with an excellent efficiency in seafloor coverage. Since they can also record the intensity of the echoes (giving indications about the seafloor nature and fine structure) they are today the favourite tool for seafloor surveys, and are a very dynamic sector of technological research.

Unlike seismic sources used in offshore exploration for seafloor investigation, and large and powerful active sonars used in military applications for submarine detection, echosounders are usually considered to cause little direct impact to the marine organisms, thanks to their high spatial selectivity and high-frequency range [2,3]. However concern has been growing recently [4] about the possible impacts caused to marine mammals (MMs) by their use, raising the perspective that MBES, if considered as harmful sound sources, should be imposed with the same mitigation procedures generally applied today by both the navies and the oil industry in their activities involving low-frequency sources. Considering the huge importance of MBES systems in today's exploration, monitoring and management of the oceans, the variety and richness of their application fields, and the scarcity of observations of their negative impacts on MMs, such a perspective requires careful preliminary analysis.

In this context, and along with recent efforts by regulators to improve the guidelines for assessing the effects of anthropogenic sound on marine mammals [5], it is essential that a clear understanding of the acoustic characteristics (radiation patterns, source

E-mail address: Xavier.Lurton@ifremer.fr

http://dx.doi.org/10.1016/j.apacoust.2015.07.012
0003-682X/

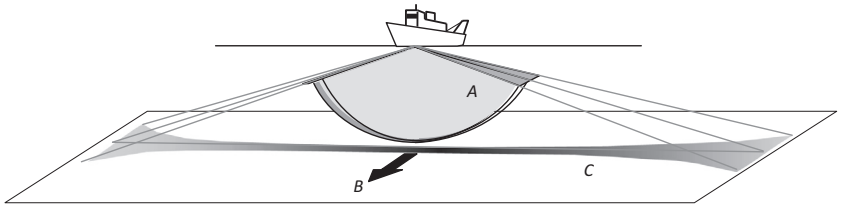

Fig. 1. The radiation pattern of a MBES features one or several (two are sketched here) transmit sectors (A), very wide across-track (typically ±70° or more) and narrow along-track (aperture 0.5–2°, according to the system model and configuration). The projection of a sector on a horizontal plane (C) is a narrow stripe perpendicular to the ship's heading direction (B) and widening at the swath ends.

levels, pulse lengths, etc.) of these systems be made widely available. Detailed studies of the impacts of active navy sonars and seismic sources have been carried out for many years [6]. Along with these studies several numerical tools (NEMO [7], ESME [8]) have been developed, combining models of acoustic propagation and MMs distributions, in order to understand the interaction of acoustic sources with animal populations; they have been made available for users to determine the potential impact needed when applying for "incidental take permits" [9] for the authorization process applicable in the USA. Each of these models requires, as a computation input, an accurate description of the acoustic characteristics of the sound source being evaluated. While such engineering descriptions have now been developed for seismic and active navy sources, there are not yet publically available models of the characteristics of multibeam sonar systems – aimed at an audience wider than specialized engineers.

The goal of this paper is hence to provide the reader and the broader community with accurate descriptions and magnitudes of the elements useful for understanding and possibly estimating the sound radiation by MBES, in the context of their potential impact on MMs. After an overview of the analysis, the fundamentals of MBES working principles (in transmission) are presented, giving the notions and practical characteristics of source level, directivity patterns, and emitted pulses. The next chapter couples these notions with a basic propagation model (whose limits are discussed) and proposed simulations of the radiated field of a few archetypes of MBES, expressed within the context of the two metrics of the maximum received Sound Pressure Level (SPL) and the Sound Exposure Level (SEL) commonly used in today's studies of sound impact to MMs [9]. The last part of the paper proposes an approximated model for estimating analytically the *SEL* accumulated during survey lines, under simplifying hypotheses regarding mainly the transmission (Tx) radiation pattern; the model is then applied to a case study of a low-frequency MBES in deep water.

The possible impacts of MBES signals on MMs in terms of physiological or behavioural effects are not addressed for themselves in this paper, which is written strictly from an engineering point of view. The goal here is to provide an appropriate objective starting point for MBES radiation modelling, usable to determine the potential insonification levels of marine animals by these echosounders.

1.2. SL, SPL and SEL

The field radiated by an acoustic source, with respect to its potential impact on marine living organisms, must be expressed [5,10] both in terms of instantaneous maximum of received pressure (Sound Pressure Level, or SPL) and cumulative intensity (Sound Exposure Level, or SEL). This implies accounting for the source nominal transmitted sound level, its frequency (defining both its harmfulness and its propagation losses), its spatial distribution (angular directivity), and its temporal characteristics (pulse duration and repetition frequency). Obviously, the received sound field also depends on several propagation phenomena (transmission losses and multipath structure).

The approach proposed along this paper is based on a simple expression of the "sonar equation". Widely used in underwater engineering, the sonar equation is an energy budget between transmitted, received and processed sonar signals [1,11,12]. Relevant forms of SPL and SEL for the present purpose are:

$$\begin{aligned} SPL(R) &= SL + DF - TL(R) \\ SEL(R) &= SL + DF - TL(R) + ED \end{aligned} \tag{1}$$

Expressed in dB (deciBels), the Eq. (1) feature the various following terms:

- *SL* is the source level, defined as the maximal value (according to angle) of acoustic pressure at $R_0 = 1$ m from the source, in dB re 1 μPa at 1 m. *SL* is usually expressed by its RMS value; one should add 3 dB if a peak value is requested;
- $SPL(R)$ is the level of acoustic pressure received at range R, in dB re 1 μPa; it is normally a RMS value, but can be changed into a peak value, similarly as *SL*;
- $SEL(R)$ is the Sound Exposure Level at range R, given by the integration of received intensity over the exposure time, simplified into the integration of the squared pressure – hence expressed in dB re 1 μPa^2 s;
- *DF* is the directivity function of the source, describing the spatial distribution of transmitted intensity; conventionally $DF = 0$ dB in the maximum intensity direction corresponding to the above definition of *SL*;
- $TL(R)$ is the transmission loss at range R during the signal propagation in the ambient medium; it features [1,12] both a geometrical term (spherical loss, or multipath summation) and an absorption term, whose influence increases very strongly with frequency;
- *ED* expresses the exposure duration effect caused by the accumulation of energy received over time; it can be roughly modelled as $10\log T$ if T is the cumulative duration of exposure (in s) of the receiving organism to a signal of constant amplitude.

The Sound Exposure Level is defined as the time integration of the squared acoustic pressure:

$$SEL = 10\log\left[\int p^2(t)dt\right] \tag{2}$$

So for one single sine-wave ping of constant maximum amplitude p_0 over a duration T, it is simply:

$$SEL_1 = 10\log[p_0^2 T/2] = 10\log[p_0^2/2] + 10\log T = SPL + ED \tag{3}$$

where *SPL* is a RMS value. For a series of pings, the *SEL* value has to be accumulated in order to integrate the received energy along time. For instance, considering a series of N pings received with the same level *SPL* at a given range, the cumulative SEL_N should be written as:

$$SEL_N = SEL_1 + 10\log N \tag{4}$$

For more general configurations where the received level varies from ping to ping, the cumulative SEL_N should be computed from

the integration of the energies of the successive pings (for this computation, the SEL has to be expressed in natural values, hence in μPa^2 s).

Some limitation has to be imposed on the integration duration: otherwise the SEL could increase indefinitely without practical significance. Since it is obviously impossible to define relevant duration values adapted to any source, receiver and configuration, such a definition has to be conventional. Two commonly-met standardized durations are one hour and 24 h; see a discussion of this issue in [5]. In the following, we will consider only the case of a single transmitted ping, and of an unlimited survey line; in both cases, specifying duration for SEL integration is unnecessary.

1.3. Preliminary remarks about sound radiation by MBES

Some initial general observations are in order at this stage, regarding MBES characteristics with respect to their potential impact on MMs:

- MBES frequencies range usually from 10 kHz to 1 MHz, corresponding to their various application domains in terms of water depths. It should be noted that the auditory frequency range [13,14] of mysticetes (baleen whales) is thought to lie below an upper limit of 10–20 kHz (depending on species) down to a lower limit of a few Hz to a few tens of Hz; while for odontocetes (toothed whales) the optimal auditory bandwidth is in the range from 10 kHz to 100 kHz, with a high-frequency cut-off at 150–180 kHz (also species-dependent). So one can consider that the potential impacts of MBES to MMs concern mainly odontocetes, for systems between 12 and 150 kHz.
- The source levels of MBES may reach relatively high values (see below); although lower than the levels observed with seismic airguns and naval sonars, they can still be considered as powerful sources compared to most underwater acoustic systems.
- The duration of transmitted signals is short, with a magnitude around the millisecond (ranging from tens of microseconds to tens of milliseconds, according to systems and operation conditions). The pulse rate frequency strongly depends on the local water depth, while the duty-cycle (*i.e.* the average proportion of time occupied by transmission) is typically of the order of a few thousandths; obviously a low duty-cycle value implies a lesser sound exposure duration for marine animals.
- The transmit directivity pattern of MBES is usually very wide in the across-track direction, and very narrow along-track (see Fig. 1). Typically the narrow-aperture magnitude currently met today is 1° (0.5–2°). Compared to wide-aperture (possibly omnidirectional) low-frequency naval or seismic sources, this implies an instantaneous coverage smaller by (roughly) one hundred times, with a corresponding decrease in the probability of having animals present inside the transmitted beam.

While the above considerations regarding marine mammals and echosounders have been well-known for some time, there has been limited published literature on the subject [2,3]. The intent of the present paper is to provide some details of description and modelling, aiming at documenting more accurately these various points.

2. Presentation of MBES transmission characteristics

2.1. Signal frequency and spectrum

2.1.1. Nominal frequencies

The frequencies of the various MBES systems available today correspond to different domains of operation. The low-frequency systems (typical frequencies 12; 24; 32; 50 kHz) are designed for deep water, thanks to the limited effect of seawater absorption in their frequency range (see Table 1). The 12-kHz systems are dimensioned for being able to map the deep oceans (4000–6000 m) and reach the greatest depths (~11,000 m) on the planet. The 24- to 30-kHz MBES class is devoted to intermediate water depths and continental slopes. The large wavelength values associated with low frequencies impose long arrays (typically $L \approx 8$ m for a 1° aperture at 12 kHz), which makes them heavy (and costly) systems restricted to high-sea vessels (which is by the way coherent with their deep-water specialization).

Medium-frequency MBES systems (typical frequencies 70; 100; 150 kHz) are designed for shallow- to intermediate-depth mapping, such as continental shelf, with water depths down to 200 m, although the lower frequencies can be used effectively on the continental slopes down to depths 500–1000 m. Their typical transducer size is sub-metric, and they can be installed on vessels of moderate size – although they are also commonly found on high-sea vessels, usually in complement to a low-frequency MBES.

Higher-frequency MBES systems (200 kHz and above) are designed for shallow to very-shallow water-depths (a few meters to tens of meters), or equivalently low altitudes above the seafloor (since they are often installed today on underwater vehicles, ROVs or AUVs, thanks to their small transducer dimensions). Several of the today's commercial systems are multi-frequency – either used for different ranges with dedicated Tx projectors, or able to transmit significantly different frequencies with the same Tx projector. The current nominal frequencies are 200, 300, 400 and 450 kHz; however some recent MBES systems propose frequencies up to 700 kHz and above.

Table 1 gives, as a function of frequency, representative values of the in-water absorption coefficient, and the array length for a beamwidth of 1°.

2.1.2. Pulse shape and duration

2.1.2.1. Classical narrowband pulses. Most often, the pulses transmitted by MBES are CW (continuous wave) signals – i.e. a sine wave at the nominal frequency, time-limited by an amplitude envelope, which is often for simplicity, considered as "boxcar" shaped, but usually has a smoother envelope, either on purpose, or the result of the frequency bandpass response of the transmitter electronics and transducer. The frequency bandwidth W occupied by a CW pulse is roughly equal to the inverse of the pulse effective duration T_P, in $W \approx 1/T_P$ (with W in Hz and T_P in s). Some acoustical energy is, however, present outside the nominal bandwidth of the signal spectrum; indeed it should be noted [16] that any finite-duration signal always has a frequency spectrum spreading over the complete frequency range – although most of the energy is (by definition) concentrated inside the effective bandwidth. It could be an interesting issue to investigate the low levels associated to the spectrum outside the nominal bandwidth. However this effect, of secondary concern, is not considered in this paper, which concentrates on the nominal frequency range of the MBES signals.

Several trade-offs occur in the optimized design of a MBES transmitted pulse. For best resolution of the measurement (bathymetry or reflectivity imaging) it may seem preferable to use as short a signal as possible. However a shorter signal corresponds to a wider frequency bandwidth, which must be compatible with

Table 1
Typical values for the absorption coefficient in seawater (α in dB/km, computed for zero depth, temperature 13 °C, salinity 35 p.s.u. according to [15]); and approximate length (L in m) for a shaded array with a beam aperture of 1°.

f (kHz)	12	24	30	70	100	150	200	300	450
α (dB/km)	1.2	4.3	6.4	24	36	50	61	80	114
L (m)	8	4	3.2	1.4	1	0.7	0.5	0.3	0.2

the passband practically acceptable by the transducer; this leads also to widen the receiver bandpass filter, hence causing an increase in the noise power received inside this band. Moreover a shorter signal defines a smaller footprint on the seafloor, decreasing the backscattered response. These two effects tend to lower the signal-to-noise ratio (SNR) obtained with short signals, which is detrimental to the measurement quality; hence a trade-off must be found.

Practically the pulse duration transmitted by a given MBES varies as a function of the system and conditions of use. For low-frequency MBES, the pulse duration ranges typically between 2 and 20 ms; the longer pulse lengths are of course reserved to longer ranges, since they provide a wider footprint on the seafloor and a narrower frequency bandwidth, both improving the signal-to-noise ratio (SNR). At higher frequencies, shorter pulse lengths can be used, approximately inversely proportional to the frequency. A good order of magnitude to consider for the pulse duration of a MBES is between $20/f_0$ and $200/f_0$ where f_0 is the carrier frequency. For instance, for a 100-kHz MBES, typical pulse durations should range between 0.2 and 2 ms.

In the case of a multi-sector transmission (Fig. 2), the various sectors are normally shot one after the other. This tends to increase the total transmission duration of the MBES. However this is hardly perceived as such by a receiver positioned in a given direction, due to the angle and frequency specialization of the sectors: the resultant exposure is dominated by the contribution of only one "well-pointed" sector.

2.1.2.2. Modulated pulses. For the purpose of increasing their operational reachable range, some MBES are able to transmit modulated signals, which are normally frequency-modulated (FM signals, often called "chirps"). The purpose of this modulation is to increase the SNR in reception [16], while providing high resolution for the time signal at the receiver output (the processing applied, based on time correlation, is commonly known as "pulse compression"). In the context of the present paper (devoted to MBES radiation), the main consequence of FM-transmission is to increase the signal duration and hence the SEL. Practically the maximum duration of FM-signals of current MBES systems does not exceed 100 ms. The bandwidth occupied by a chirp is well approximated by the extent of the frequency sweep.

In multi-Tx sector MBES, the transmission of FM signals is primarily applied to external sectors (where the oblique-range limitation appears first); it is possibly extended to the inner sectors for use in very deep waters.

2.1.3. Multi-frequency spectrum

In case of a MBES with multiple Tx sectors, the total frequency spectrum occupied at transmission can be simply considered as the combination of the individual spectral contributions of the signals transmitted in the various sectors; hence it depends on:

- The values of nominal frequencies transmitted in the different sectors;
- The individual spectrum associated to the time signals.

The frequency bands associated to time signals are conventionally defined by their bandwidth measured at −3 dB; however, this strict spacing is not wide enough to avoid overlapping of the multi-frequency spectrums and may generate crosstalk between sectors; hence a wider spacing between the frequency components is to be met in the actual frequency band occupation.

2.2. Source level

The source level (*SL*) is the maximum pressure value (according to angle) radiated by the transmitter. For sonar signals, it is expressed in dB re 1 μPa RMS (hence, for a constant-amplitude CW pulse, which is a correct approximation for MBES signals, it is 3 dB below the signal peak value).

Consider a line array of equally-spaced transducer elements. The maximum source level is then proportional to the array length L for a given individual electrical power applied to each of the transducer elements. Moreover the main lobe of the directivity pattern has a width approximately equal to (λ/L) where λ is the acoustical signal wavelength [16]. So the effect of increasing the array length is twofold: it increases proportionally the total electrical power at the input and hence the radiated acoustical power; and moreover the acoustical intensity radiated in the main lobe is increased by the narrower focusing of the transmitted sector. Finally the *SL* value in dB shows a $20\log L$ dependence: e.g. doubling the array length increases the available maximal *SL* value by $20\log(2) = 6$ dB (3 dB for doubling the electrical power and 3 dB for halving the lobe aperture). Several manufacturers support different Tx array lengths for their MBES (especially the low-frequency systems), corresponding to various Tx apertures along-ship; this is made possible by the modular design of these arrays.

The *SL* of low-frequency systems is usually higher than for high-frequency systems. This has to do with the emitting surface of the transducers, making more power available for the large arrays needed in low-frequency to get angular narrowness. Low-frequency MBES (12 kHz) may radiate instantaneous levels as high as 240 dB re 1 μPa at 1 m, and exceptionally more. High-frequency MBES do not normally exceed 215–220 dB re 1 μPa at 1 m.

For a MBES, the maximum pressure value is obtained either in the vertical direction below the carrier vehicle, or along two

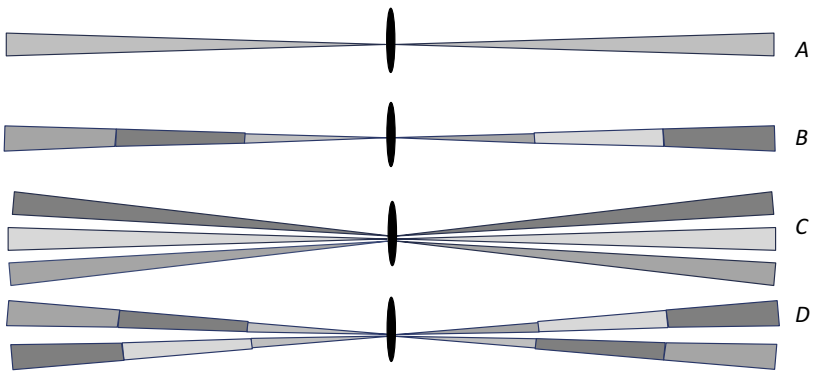

Fig. 2. Schematic examples of MBES transmission sectors projected on a horizontal plane, according to the Tx array design. (A) Single sector and frequency; (B) Multi-sector, single swath (here 6 freq.); (C) Single sector, multi-swath (here 3 freq.); (D) Multi-sector, multi-swath (here $2 \times 6 = 12$ freq.).

oblique across-track directions symmetrical to the vertical. This depends on the Tx array hardware structure, and on its transmitting configuration.

As explained above and illustrated in Fig. 2, some systems are able to transmit in several across-ship sectors through a beamforming processing. This implies a matrix-geometry of the array, with several rows of transducer elements along the transmit array length – making it possible to form beams thanks to the array width. In this case, the same *SL* value can theoretically be obtained successively inside the various sectors. However the actual level may be different, due to the angular directivity of the transducer elements (see next paragraph) and to their sensitivity variation with frequency.

It should be noted that the source level of a sonar antenna is normally defined by its radiation in the "far field" [1]; in this regime all the array elements contribute coherently to the resultant field, and the range dependence of the pressure amplitude is inversely proportional to the oblique range *R*, as for an equivalent spherical source. However at short enough ranges (in the "near-field" region) the summation of individual contributions creates an interference field preventing the radiated pressure field from reaching its nominal level. Hence the far-field radiation level, when extrapolated to short ranges, overestimates the actual physical level. This overestimation may reach a significant magnitude, and it is better to account for it for the realism and accuracy of the physical modelling. However, neglecting this effect is conservative in the estimation of sonar impacts of upon marine life; hence, for the sake of simplicity we will stay within this approximation along this paper, which is more focused on long-range sonar radiation than on near-field propagation phenomena.

2.3. Tx directivity pattern

2.3.1. Transmission geometry

In the following, the sound field radiated by the MBES is computed as a function of spatial coordinates. For a receiving point (see Fig. 3) at a given depth z and defined horizontally by (x, y) referenced to the Tx antenna centre (0, 0, 0), the geometrical data to consider are the oblique range R, and the along- and across-track angles φ and θ, given by:

$$\begin{aligned} R(x,y,z) &= \sqrt{x^2+y^2+z^2} \\ \varphi(x,y,z) &= \arctan(x/R) \\ \theta(x,y,z) &= \arctan(y/R) \end{aligned} \tag{5}$$

The oblique range R is used in the expression of the transmission loss. The along- and across-track angles φ and θ are used in the expression of the Tx directivity patterns expressed in the corresponding planes. The angle ψ relative to the vertical is used in the elemental transducer directivity pattern.

It should be noted that the angles used here are different from the classical spherical coordinate angles. They are primarily adapted to model the radiation directivity pattern of two ideal linear arrays disposed along the *x*- and *y*-axis.

2.3.2. Transducer element directivity

Transmitting arrays of MBES are made of a line or a matrix of transducer elements. The purpose is to give them the versatility provided by beamforming [16] and steering of multiple transmit sectors (either along- or across-ship), making possible to define a variety of transmission modes and also to compensate in real time the platform motion. The transducer elements may be either cylindrical (or toroidal), assembled in a row to form a linear array; or have a flat radiating surface (Tonpilz technology in low frequency, ceramic blocks at higher frequencies [1]) which can be grouped in a 2-D matrix. The first solution makes beamforming possible only along-track in φ angle; the second one in both φ and θ.

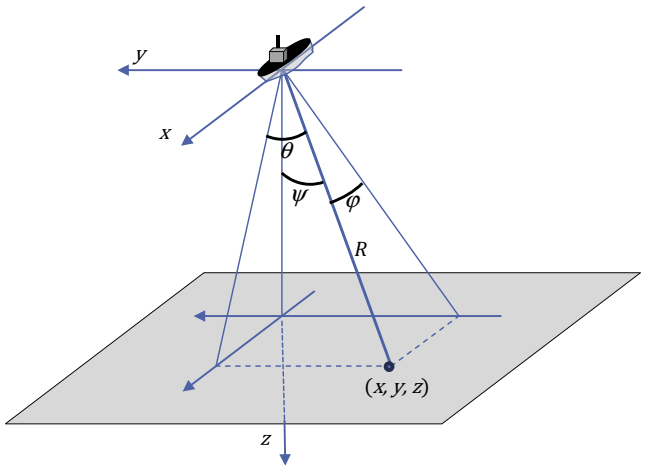

Fig. 3. Spatial geometry of the echosounder radiated field. The Tx array is located along the *x*-axis, hence its nominal maximum radiation plane is the vertical plane (*yz*).

The resulting directivity of the array is a combination of the directivity patterns of respectively the element transducers $D_E(\theta)$ and the beamforming processing $D_B(\theta)$, expressed in dB as:

$$D(\theta) = D_E(\theta) + D_B(\theta) \tag{6}$$

Regarding the directivity pattern, a Tx transducer element is expected to behave like a classical "small" source, with a very wide lobe and a slow decrease of level with angle, accelerating on the sides. Fig. 4 gives an actual example of such a directivity pattern, for a transducer element of a 30-kHz MBES flat array, measured in a water tank [17]. The total beamwidth (at −3 dB) is here about 100°; the decrease on the sides (at 90° from axis) reaches −15 dB.

It is proposed to describe here the directivity pattern of individual elements by the simple empirical form, expressed as a function of the angle ψ relative to the transducer axis (Fig. 3):

$$D_E(\psi) = 20\log\left(\left|\frac{\sin E}{E}\right|\right) \text{ with } E = \frac{\pi\psi}{\Delta\psi_E} \tag{7}$$

It has been assumed here that the directivity pattern of the elemental transducer has a cylindrical symmetry around the transducer axis; hence the same formula (7) is valid whatever the azimuth direction if the transducer axis is vertical (which is most often the case for bathymetry MBES, whose arrays usually transmit downward).

This form (7) is inspired from the expression of the main lobe of a rectilinear transducer [16], with the difference that the angle value ψ is used instead of its sine. As an approximation to the case presented in Fig. 4, choosing a value $\Delta\psi_E = 107°$ provides an actual lobe width (at −3 dB) around 100° and a decrease of −14.9 dB at 90° (see Fig. 4).

Obviously the exact directivity patterns of elemental transducers (fundamentally controlled by their physical design) observed for particular models developed by the various constructors depend on their exact geometry and dimensioning. However the simple model proposed above, with one single parameter $\Delta\psi_E$, is expected to be sufficiently representative for the purpose of building a synthetic model of MBES radiation. The accurate modelling of particular cases is out of the scope of the present study, and should be conducted according to detailed information provided by the constructors.

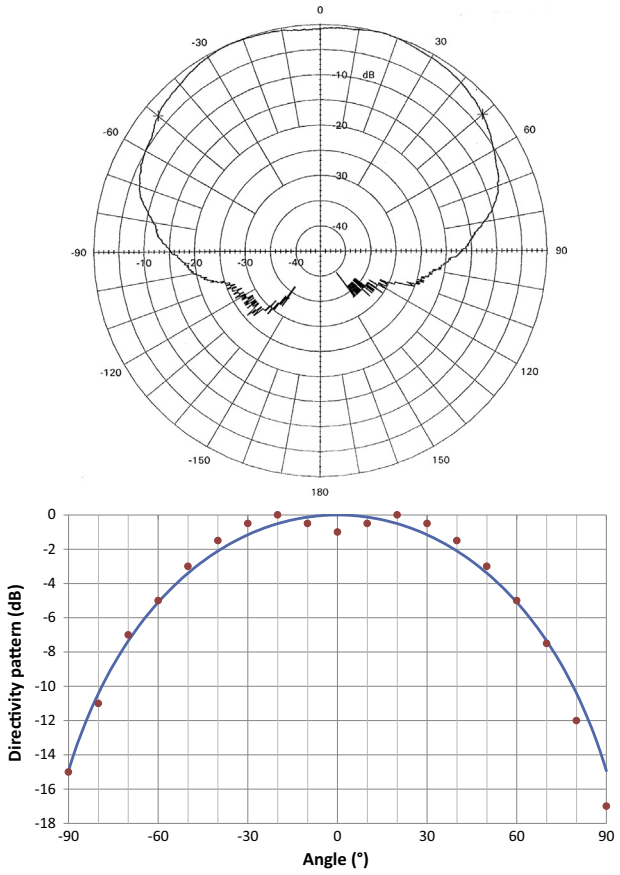

Fig. 4. (Upper) Across-track directivity pattern of Tx elemental transducer from an MBES array, measured in test tank [17]. (Lower) Modelled directivity pattern (solid line) for a 30-kHz elemental transducer from a MBES array. See Eq. (7) and parameters in the text. The dots (in red) are approximate values extracted from the upper plot. (For interpretation of the references to color in this figure legend, the reader is referred to the web version of this article.)

2.3.3. Across-track beamforming of Tx sectors

The across-ship width of the Tx array can be used for beamforming the Tx sectors, steerable across-track at various angles. For further discrimination upon reception, each sector is formed at one specific frequency, with a relatively narrow bandwidth kept inside the passing band of the element transducers. As a classical effect of beamforming, the lobe width increases with the steering angle, and the symmetry of the lobe is distorted. This multiple-sector concept was introduced as soon as the second generation of MBES, in the late 1980s, e.g. in the Simrad EM 12 [18]. Its relevance is twofold: sector focusing increases the intensity level at transmission since the available acoustic power is concentrated inside a limited angle sector; and the frequency specialization helps to limit the impact of the strong specular echo (reflected perpendicular from the seafloor interface) to a restricted part of the angle coverage thanks to the frequency separation between sectors.

Omitting here the directivity of elemental transducers described above, if the same set of Tx elements is used to form the various sectors, it is expected that no level difference appears between the maximum levels of the sectors beamformed at various steering angles. However, level shifts may be observed between sectors formed at different frequencies, depending on the frequency response of the transducers. Moreover, certain sectors can be de-focused, in order to increase their lobe width, at the expense of a decrease in the transmitted intensity level [19].

It is proposed here, for the main lobe part of the beamforming directivity pattern $D_B(\theta)$, to use the classical form of the linear array forming a steered beam [16]:

$$D_B(\theta) = 20\log\left(\left|\frac{\sin A}{A}\right|\right)$$

$$\text{with } A = \frac{\pi L_{ac}}{\lambda}(\sin\theta - \sin\theta_S) \approx \frac{\pi}{\Delta\theta_S}(\sin\theta - \sin\theta_S) \text{ for } |A| < \pi \quad (8)$$

where L_{ac} is the array length across-track, λ the wavelength, θ_S the steering angle, and $\Delta\theta_S$ the sector beamwidth (defined at -3 dB, expressed in radians). Eq. (8) has its maximum value at $\theta = \theta_S$. Also the $D_B(\theta)$ lobe shape is asymmetrical in θ around θ_S, due to the $(\sin\theta - \sin\theta_S)$ term.

Outside the main lobe, the antenna still radiates intensity through a number of sidelobes. The level of sidelobes can be controlled by a shading law applied along the array, in order to bring them below their "natural" level defined (for a line array) by the cardinal sine function inside Eq. (6). The most common shading law (Dolph–Chebyshev) is designed for keeping the maximal level of sidelobes at a predetermined value, whatever their angle, while minimizing the degradation of the main lobe aperture [20]. Although a target value for these side lobes (typically -30 dB) is defined when setting the parameters of the shading law, this ideal value is rarely obtained in practice, due to the intrinsic imperfections of the transducer elements. On the other hand, the sidelobe nominal level corresponds to the maximum of the lobes, while the mean radiated intensity value (averaged over angle) is lower, by about -3 dB. It can be considered that the two phenomena (degradation of the nominal sidelobe level; average angular value lower than the nominal value) approximately compensate each other. Finally, we will admit that the average radiated level over the sidelobes is given by their nominal value (the reader can find a short development and illustrations of this approach in Appendix A). Hence this conservative average value will be used in the following as a floor value for the beamformed sectors outside the main lobe.

Fig. 5 presents the radiation directivity model of a multi-sector generic MBES, with a set of 7 sectors defined by their steering angle ($-55°$, $-30°$, $-14°$, $0°$, $14°$, $30°$, $55°$) and their lobe width ($28°$, $18.5°$, $16.5°$, $16°$, $16.5°$, $18.5°$, $28°$). The left-side plot depicts the directivity patterns obtained by the beamforming, modelled by Eq. (8) and a floor sidelobe value of -30 dB; the right-side one combines the Tx sectors with the transducer element directivity given by Eq. (7) and Fig. 5.

2.3.4. Along-track directivity pattern

A narrow along-track Tx lobe aperture is a distinctive feature of MBES. This characteristic controls the spatial resolution of the signal footprint along-track, and hence is a paramount parameter in the performance of the system for seafloor mapping purposes. This is obtained by the operation of a long array, aligned along the carrier vehicle longitudinal axis, and processed in order to create a vertical (or close to vertical) narrow transmit lobe. The best systems in this respect today have an aperture of typically $1°$, some as narrow as $0.5°$. Minimizing the reception of unwanted echoes outside the main lobe imposes to apply array shading in order to lower the sidelobe levels.

The need for compensating the ship's motion (pitch and yaw, in order to have the swath always at the nadir of the vehicle and orthogonal to the track) requests that the Tx sector be steered in real time according to the angle measurements from the Motion Reference Unit. As steering angles are typically small values, this does not change significantly the radiation characteristics of the system.

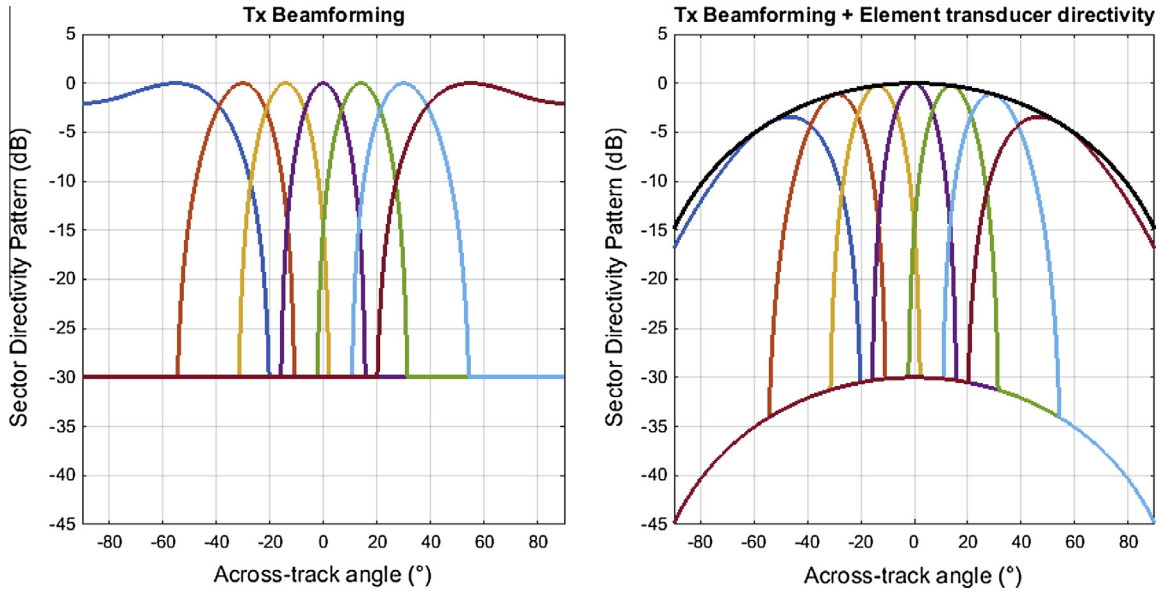

Fig. 5. Model of Tx directivity patterns for a multisector MBES. See detailed parameters in the text. (Left) Directivity patterns of the beamformed Tx sectors from Eq. (8) with a floor value of −30 dB outside the main lobe. (Right) Combination of the sectors (colours) with the individual directivity pattern (black) of element transducers. (For interpretation of the references to color in this figure legend, the reader is referred to the web version of this article.)

Multi-swath transmission (Fig. 2) modifies more significantly the radiated field: in order to increase the sounding point density, several Tx sectors can be formed along-track (up to 5 in today's state of the art), at steep angles around the vertical axis, and at different frequencies for a purpose of separability upon reception. Consequently, for every ping the insonified space is then multiplied by the number of sectors formed along-track.

For the modelling, we will consider here a Tx sector of 1° aperture (at −3 dB) radiated by a rectilinear array. The beamforming directivity pattern is combined with the directivity pattern of the transducer elements. Fig. 6 depicts these two components, and the resulting directivity pattern.

The array directivity pattern (in the main lobe) is given by:

$$D(\varphi) = 20\log\left(\left|\frac{\sin G}{G}\right|\right)$$

$$\text{with } G = \frac{\pi L_{al}}{\lambda}(\sin\varphi - \sin\varphi_S) \approx \frac{\pi}{\Delta\varphi_S}(\sin\varphi - \sin\varphi_S) \approx \frac{\pi}{\Delta\varphi_S}(\varphi - \varphi_S)$$

$$\text{for } |G| < \pi \qquad (9)$$

where L_{al} is the array length along-track, λ the wavelength, φ_S is the along-track steering angle, and $\Delta\varphi_S$ is the sector beamwidth (at −3 dB, in radians). Again, only the main lobe is considered here, down to the conservative sidelobe floor value of −30 dB. One can approximate here the angles by their sine since in this MBES geometry context the φ values inside the main lobe and the φ_S steering angles remain small.

3. Detailed modelling for a single transmission

3.1. Radiation model at 1 m

At this stage, all the elements have been made available for estimating a model of radiation expressed at the conventional reference distance of R_0 = 1 m. The received peak level $SPL(R_0)$ is given by the nominal source level SL (defined at 1 m) modulated by the directivity functions in θ and φ, augmented by 3 dB with regard to the RMS value.

The Sound Exposure Level (SEL) at the reference distance R_0 = 1 m is given by the summation of the energy contributions

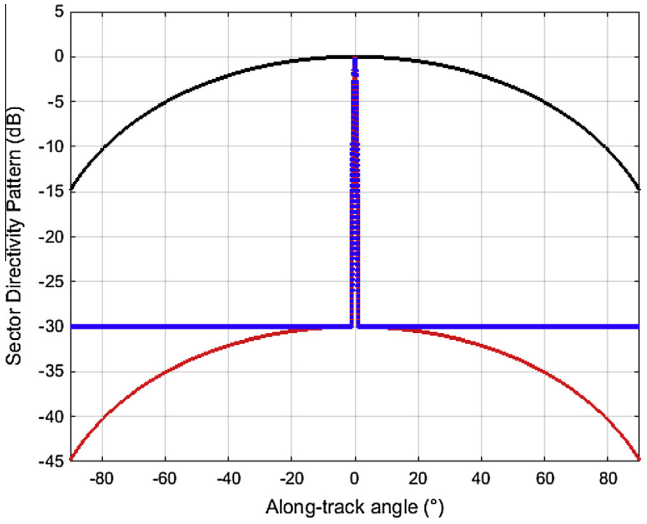

Fig. 6. Along-track radiation pattern of a 1°-wide Tx sector, for the array beamforming (blue) given by Eq. (9) and a floor value of −30 dB; the element transducers (black); and their combination (red). The (blue) and (red) plots are superposed in their central part (main lobe). (For interpretation of the references to color in this figure legend, the reader is referred to the web version of this article.)

received at R_0 as a function of angles θ and φ. It is considered here in the case of one transmitted ping. In case of a unique Tx sector, the SEL is simply given by SPL corrected by the received pulse duration T_P (in s), hence:

$$SEL(R_0) = SPL(R_0) + 10\log T_P \qquad (10)$$

In case of a multi-sector transmission, one must account for the summation of the various sectors contributions received at a given point $SEL(R_0, \theta, \varphi)$

$$SEL(R_0) = 10\log\left(\sum_n p_n^2(R_0,\theta,\varphi)T_{Pn}\right) \qquad (11)$$

where $p_n^2(R_0,\theta,\varphi)$ is the RMS squared pressure radiated inside sector n, lasting for duration T_{Pn}. The sector summation is over all

the Tx sectors activated during the ping sequence, so at a given point the contributions of the complete set of along-track multiple swaths and across-swath sectors have to be accounted for. Note that normally the Tx sectors are designed so that their main lobes do not overlap significantly, and this limits the actual impact of the summation expressed in (11); however the summation of the sidelobe contributions remains, and may impact the resulting field outside the main lobe(s).

Fig. 7 illustrates these various definitions; for the multi-sector MBES proposed above, it shows the Tx radiation at R_0 from the individual sectors and their combination for obtaining the *SL* and *SPL* values (as a maximum over all sectors) and the *SEL* (as a quadratic summation over all sectors). Note that the *SEL* computation smoothes out the modulation by the directivity lobes of the Tx sectors.

Fig. 8 depicts *SPL* and *SEL* as a function of both along- and across-ship angles. It illustrates mainly the fact that the radiation by the MBES happens in a narrow along-track angle range (yellow line on the plot), with a much lower level everywhere else.

3.2. Integration with an elementary propagation model

We apply at this point the classical propagation model for transmission losses [11]:

$$TL = 20\log R + \alpha R \tag{12}$$

combining a spherical spreading law ($20\log R$) and an absorption term (αR). This model implies that the propagation happens in free-field over a direct path of slant range R from the source to the receiver and without any effects of multipaths. The second term is caused by the absorption effect in seawater, a physical effect caused by both the fluid viscosity and chemical effects, with a strong dependence on frequency [15].

This simple model is the one traditionally used for conventional estimations of sonar performance. Its interest and popularity for detection performance estimation comes, besides its simplicity, from the fact that it usually underestimates the received intensity (because it considers one single direct path instead of a multipath combination), hence providing conservative estimates in terms of target detection. Conversely, for the topic of radiation level prediction and impact evaluation, the underestimation of the received intensity can be detrimental.

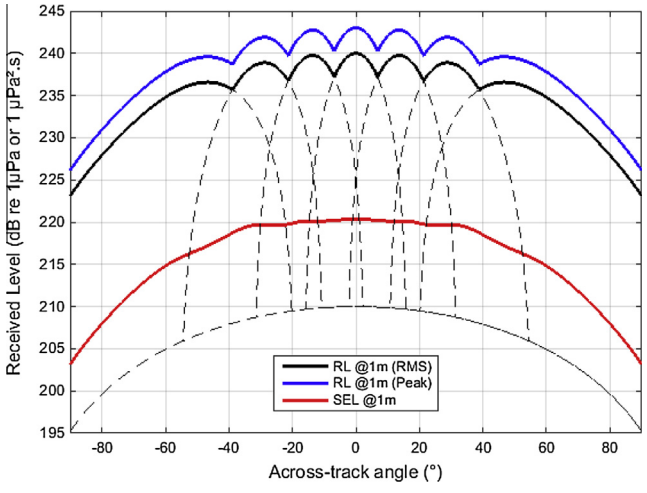

Fig. 7. Plot of the radiated field at 1 m as a function of the transverse angle θ. The plot features the individual beam patterns of the beamformed sectors (dashed lines, with a sidelobe floor value at −30 dB) compensated for the element transducer angular response; the effective resultant *SPL* = *SL* + *DF* (black), as the maximum RMS value of the sectors; the peak received level (blue) which is increased by 3 dB above the RMS level; and the SEL (red) for a 10-ms pulse duration, which is given, for each angle, as the summation of the individual sector contributions. (For interpretation of the references to color in this figure legend, the reader is referred to the web version of this article.)

However, in many configurations the direct path contribution dominates the field components reflected on the seafloor and sea-surface; hence a single-path simplification gives acceptable orders of magnitude for rough estimations. In the MBES-radiated field, there is however an important exception at angles grazing to horizontal. In this case the direct field is strongly attenuated by the Tx directivity pattern collapsing (see Figs. 9–11). The field reflected by the seafloor may then dominate the direct radiation; this issue is addressed below in a dedicated section below (Section 4.5).

3.3. Application to MBES case studies

3.3.1. Configurations

The radiated field, computed from echosounder characteristics (source level, pulse duration, directivity patterns) and a propagation model, can finally be plotted both in the vertical and the horizontal planes. Several examples are presented here.

Assuming no pitch-related effect and no along-track steering of the Tx sector, the vertical plane corresponds to the highest insonification level inside the water column. Alternatively, the field can be plotted over several horizontal planes at various depths. This type of presentation illustrates the effect of the along-track narrow aperture as well as multi-sector configuration.

Three "generic" MBES systems are considered here. None of them is strictly an actual commercial system; however their characteristics are representative of current models operated today.

MBES #1 is a high-frequency system (100 kHz) devoted to continental shelves (down to 200 m), with a simple structure of one Tx sector both along- and across-track. MBES #2 is a medium–low frequency system (30 kHz), representative of MBES (24–36 kHz) usable in medium-to-deep water for high-resolution applications; it features three along-ship Tx sectors and only one sector across-ship. MBES #3 is a low-frequency system (12 kHz) usable in deep to very-deep water for large-scale mapping; it features seven Tx sectors across-track and only one sector along-ship, and was already considered in the previous sections.

The geometrical configurations used for the computations depend on the MBES characteristics, and are also representative of the MMs dive depths. For MBES #1 we chose depths of 20; 50; 100; and 150 m; for MBES #2 100; 500; 1000; and 1500 m; and for MBES #3 100; 500; 1000; and 2000 m.

The values of the absorption coefficients are the ones given in Table 1. They are to be considered as conventional values, since (1) they may vary according to the local oceanographic conditions and (2) they do not feature the depth (or hydrostatic pressure) dependence, which may be very significant in deep water.

3.3.2. Radiated field results

For each one of the generic MBES considered here, the radiated field is first displayed in the across-track vertical plane (upper part of Figs. 9–11). It is presented under two forms: the maximum sound pressure amplitude (maximum peak value over the various Tx sectors), and the SEL (RMS summation over the various Tx sectors, including the sidelobe contributions). Note that in case of along-track Tx multi-sectors, the vertical plane presented here is actually a "quasi-vertical" one, approximating the along-ship tilt from vertical to zero. The field level (coded in colors) is completed by series of iso-level lines (by 10-dB steps). In a second series of plots (lower part of Figs. 9–11), the radiated field (in SEL) is presented in the horizontal plane, at four different depths.

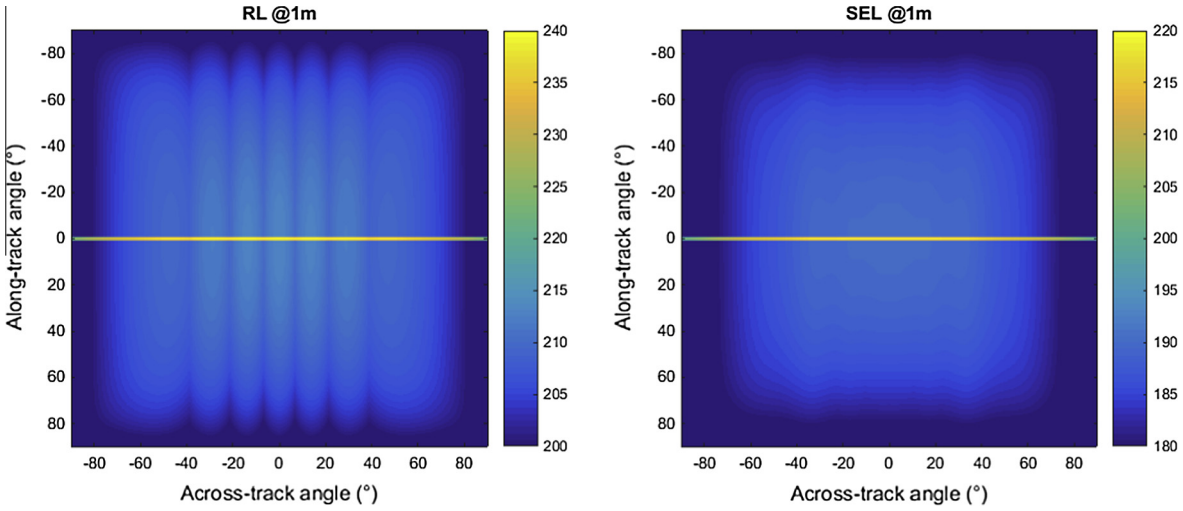

Fig. 8. Plot of the radiated level *RL* (left, color bar in re 1 μPa at 1 m) and *SEL* (right, color bar in re 1 μPa^2 s at 1 m) as a function of the across- and along-track angles (θ, φ). (For interpretation of the references to color in this figure legend, the reader is referred to the web version of this article.)

It can be observed that the general shape of the radiated field does not vary much. In the vertical plane, it is mainly controled by the individual transducer directivity; the Tx-sector modulation is clearly visible in the SPL plots, and rather smoothed out in the SEL (see Fig. 7). In the horizontal plane, the radiation pattern is concentrated inside the narrow main lobe (duplicated along-track for MBES #2); everywhere else is the low-level radiation by sidelobes, modulated by the individual transducer directivity (see Fig. 8), and at a lesser extent by the beamformed Tx-sectors.

3.3.3. Ranges corresponding to impact thresholds

A simple analysis is applied here to quantify the magnitude of the minimum ranges corresponding to conventional impact threshold values. From the paragraphs above, it is understood that:

- The maximum received level SPL_{max} is observed inside a Tx lobe, along the main axis. It can be obtained from the constructor's specifications.
- Along a survey line, the cumulative SEL is a combination of contributions from both the Tx main lobes (highly energetic but rarely active at one given receiving point, due to their directivity narrowness) and the sidelobes (with low levels, but systematically perceived because of their wide-angle radiation).

Using the notations of Eq. (1), the received level threshold value SPL_{Thr} is obtained at a range R_{ThrSPL} given by:

$$SPL_{Thr} = SL_{Peak} + DF - TL(R_{ThrSPL}) \quad (13)$$

The source level to consider is the peak value (+3 dB above the nominal RMS value *SL*) in the Tx lobe axis, hence with a *DF* term taken at 0 dB. The transmission loss comes as:

$$TL(R_{ThrSPL}) = 20\log(R_{ThrSPL}) = SL_{Peak} - SPL_{Thr} \quad (14)$$

Approximating the transmission loss by the only spherical divergence is justified at short ranges, when the effect of absorption can be neglected; this can be checked in the results (see Fig. 12).

A similar approach is applied to the SEL associated with a single ping of duration T_p:

$$SEL_{Thr} = SL + 10\log T_P + DF - TL(R_{ThrSEL}) \quad (15)$$

$$TL(R_{ThrSEL}) = 20\log(R_{ThrSEL}) = SL + 10\log T_P - SEL_{Thr} \quad (16)$$

In both (13) and (15) only the main lobe radiation is considered, since for one single ping the sidelobe contribution is comparatively negligible.

The threshold values are taken from [10]. Two criteria are considered (injury and behavioural response), each one expressed as SPL and SEL. The cetacean species are grouped inside three families, however the numerical values are identical for the three families. The pinnipeds form one different class, with threshold values 12 dB below the cetacean values. Table 3 summarizes the key figures of this analysis. It should be noted that all these values correspond to single-ping exposure configurations; no simple value can be given for the behavioural response criteria corresponding to multiple-ping configurations.

The dependence of the threshold range is given in Fig. 12, as a function of the nominal source level with $T_P = 0.01$ s, both for injury (left) and behaviour (right) criteria. Considering the injury criteria, the results illustrate that injury hazards are possible only at very short distances from the source: e.g. about 5 m for SPL and 12 m for SEL in the case of a 240-dB source level, considering cetaceans. For behavioural response criteria, the corresponding values are 9 m and 70 m. For pinnipeds, all ranges are multiplied by a factor of 4.

All these results are conservative, since (1) they assume that the receiver has actually been reached by a Tx main lobe; (2) they approximate the insonification level by its far-field value, which overestimates the near-field level at the short ranges obtained here; (3) they neglect the directivity and absorption phenomena, the effect of which is to decrease the intensity at the receiver.

A similar analysis will be conducted in a next section, using a more complete radiated field model.

4. Simplified modelling for application to survey configurations

4.1. Approximated radiation model

After having accurately detailed the radiation by MBES systems, the purpose is now to propose a simpler model for the practical estimation of the radiated field in common cases of seafloor-mapping surveys. At sea, the coverage of an area of interest is normally done as a network of parallel lines, spaced by a conventional swath width whose actual extent may depend on the expected quality of the resulting data (some overlapping is usually

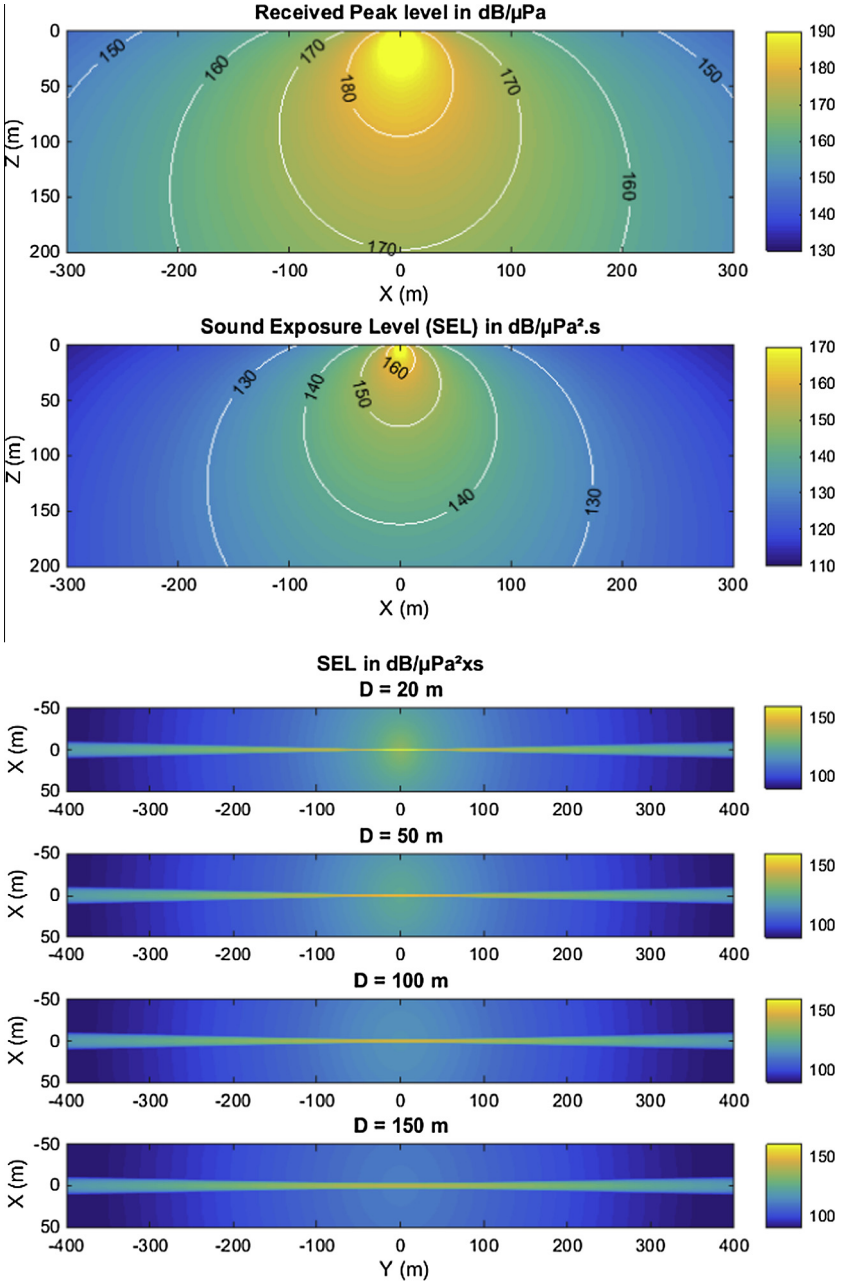

Fig. 9. Radiation pattern for the case of MBES #1. The upper part depicts the field in the vertical plane plotted as the peak amplitude SPL value (upper) and the Sound Exposure Level SEL (lower). The lower part gives horizontal crosscuts of the SEL at depths (20; 50; 100; and 150 m).

applied). We will not get here into a discussion about coverage strategies, and the following will consider the simple case of one straight survey line over a flat and horizontal seafloor.

A number of assumptions and approximations will be made. The survey line is run at constant speed, and the sonar pings at a stable rate. The receivers are supposed to be fixed, i.e. at a given observation point the cumulative intensity depends only on the MBES motion.

The radiation by the MBES is described using a simplified approach. The directivity pattern used for Tx array beamforming is approximated by an ideal angular shape $D_A(\theta, \varphi)$, with a constant amplitude vs angle inside the equivalent effective beamwidth [1], and a constant sidelobe level elsewhere. This beamforming directivity is modulated by the element directivity $D_E(\psi)$. Hence, expressed in dB:

$$\begin{aligned} &D_A(\theta,\varphi) = D_S(\theta,\varphi) + D_E(\psi) \\ &D_S(\theta,\varphi) = 0 \text{ dB for } |\varphi| \leqslant \frac{\Delta\varphi}{2} \text{ and } \forall\theta \\ &D_S(\theta,\varphi) = -B \text{ dB elsewhere} \\ &D_E(\psi) = 20\log\left(\left|\frac{\sin E}{E}\right|\right) \text{ with } E = \frac{\pi\psi}{\Delta\psi_E} \end{aligned} \tag{17}$$

Expressed in terms of sound level, it can be said that the radiated level at 1 m in a given direction is either SL_{ML} inside the main lobe(s); or $SL_{SL} = SL_{ML} - B$ inside the sidelobe region. With this notation, SL_{ML} and SL_{SL} have to be corrected for the element directivity pattern $D_E(\psi)$.

For a multi-sector MBES, it is assumed that the Tx sectors inside the swath are ideally filling in the total angular coverage without overlapping (Fig. 13).

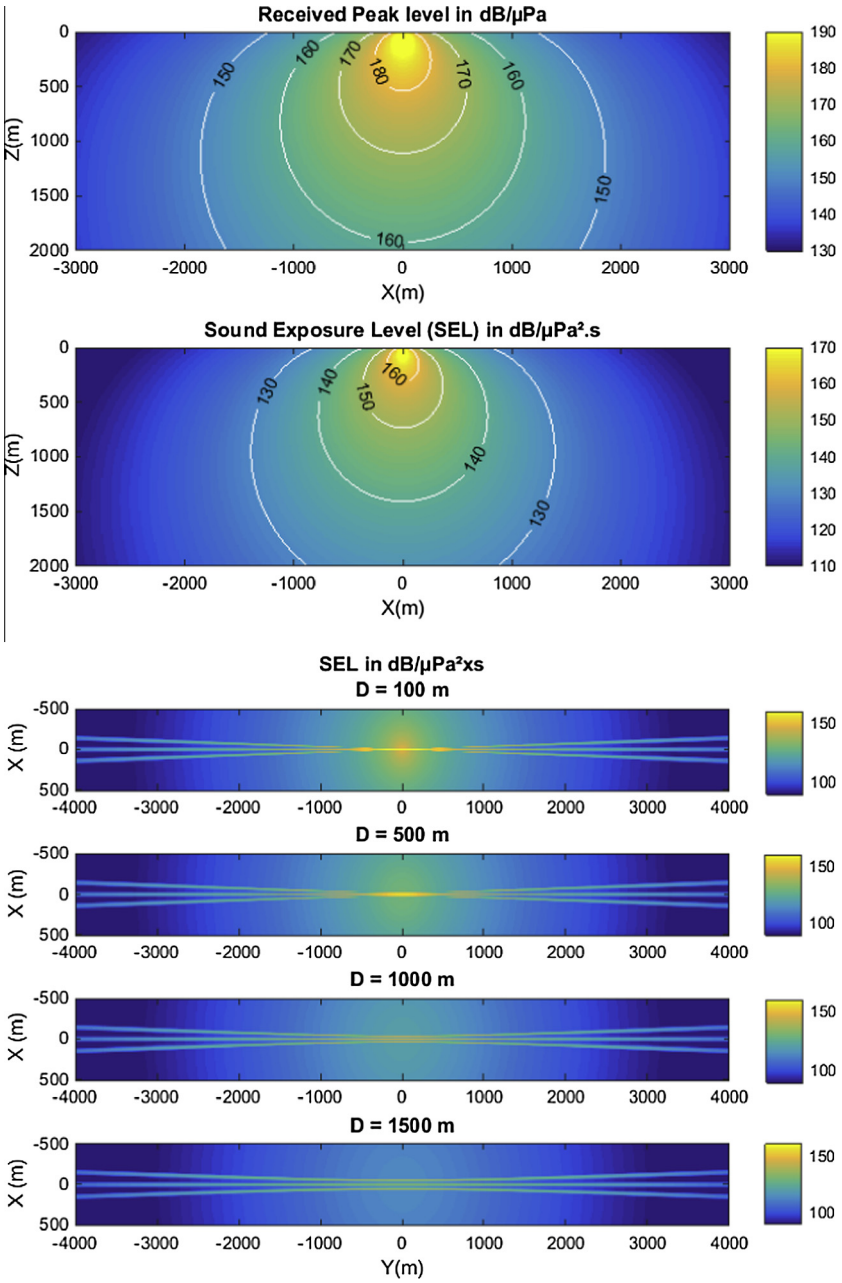

Fig. 10. Radiation pattern for the case of MBES #2. The upper part depicts the field in the vertical plane plotted as the peak amplitude SPL value (upper) and the Sound Exposure Level SEL (lower). The lower part gives horizontal crosscuts of the SEL at depths (100; 500; 1000; and 1500 m).

4.2. Radiation from one single ping

4.2.1. Maximal received level

Going back to the elementary model given in Section 1.2 for the SPL and SEL, and the approximated directivity pattern (15), the received level at a given point at range R and direction ψ is given by:

$$\begin{aligned} SPL_{ML} &= SL_{ML} - 20\log R - \alpha R + D_E(\psi) \\ SPL_{SL} &= SL_{SL} - 20\log R - \alpha R + D_E(\psi) \end{aligned} \tag{18}$$

respectively in the main lobe and in the sidelobes, and depending only on the insonification geometry controlling the transmission loss and directivity.

4.2.2. Sound Exposure Level

For a single-sector MBES, the SEL in the main lobe and in the sidelobes is obtained by accounting for the pulse duration T_p in Eq. (18):

$$\begin{aligned} SEL_{ML} &= SL_{ML} + 10\log(T_P/R^2) - \alpha R + D_E(\psi) \\ SEL_{SL} &= SL_{SL} + 10\log(T_P/R^2) - \alpha R + D_E(\psi) \end{aligned} \tag{19}$$

For a multisector MBES (along- or across-track), the SEL should account for the cumulative contributions of the various Tx sectors. Inside the main lobes, this should not change significantly the SEL: the main-lobe field of one sector is hardly increased by the sidelobe level of the other ones. But in the sidelobe area, the resultant SEL is a combination of all contributions from the various Tx sectors (be it along- or across-ship); assuming the same sidelobe level

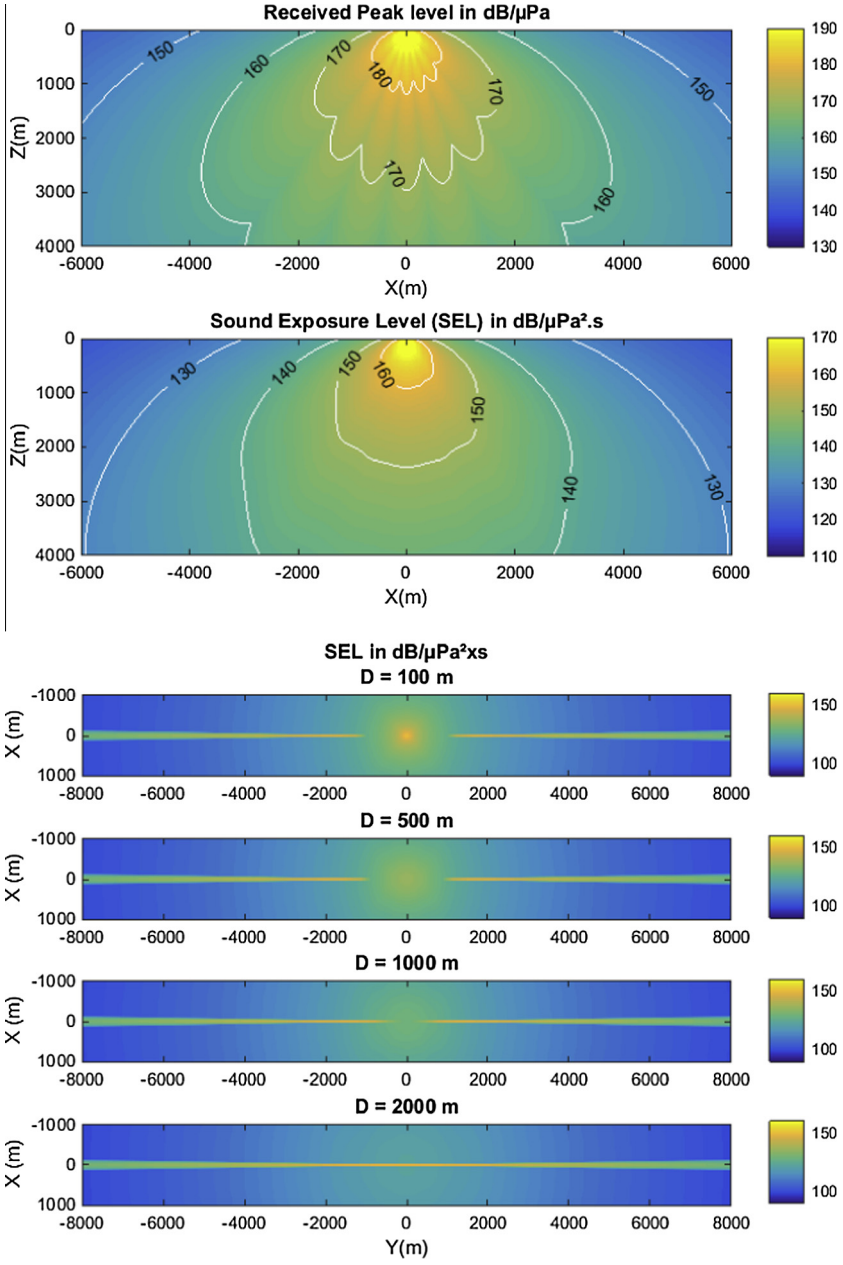

Fig. 11. Radiation pattern for the case of MBES #3. The upper part depicts the field in the vertical plane plotted as the peak amplitude SPL value (upper) and the Sound Exposure Level SEL (lower). The lower part gives horizontal crosscuts of the SEL at depths (100; 500; 1000; and 2000 m).

for all the sectors, then the SEL is increased by $10\log N_s$, where N_s is the total number of Tx sectors. So for a multi-sector MBES, the SEL (respectively inside any one of the main lobes, and outside the main lobes) is given by:

$$\begin{aligned} SEL_{ML} &= SL_{ML} + 10\log(T_P/R^2) - \alpha R + D_E(\psi) \\ SEL_{SL} &= SL_{SL} + 10\log(T_P/R^2) - \alpha R + D_E(\psi) + 10\log N_S \end{aligned} \tag{20}$$

4.3. Cumulative exposure along a survey line

At a given receiving point and for a sonar in motion along a survey line, insonification by the main lobe(s) is controlled by the lobe width at the range considered, since the insonified volume widens with the distance from the source (see Fig. 14). For a series of regularly-spaced pings along the ship's route, a given receiver can be insonified either 0–1 time if its orthogonal range Y to the line is smaller than Y_1; or 1–2 times at ranges between Y_1 and Y_2; etc. Usually, due to the narrowness of Tx sectors, the number of effective pings reaching the receiver within the main lobe is expected to be quite small, and with little differences of level between the successive pings received. Hence the *SPL* value is then obtained in a very straightforward way, as its expression at the minimal transmission loss and maximal directivity pattern. The *SEL* is given by its value for one ping increased by a limited number of effective pings.

The modelling of the cumulative *SEL* due to sidelobes is obviously different, since the horizontal angle selectivity prevalent for the main lobe cannot be applied. If the sidelobe regime is considered to radiate homogeneously in the horizontal plane, then a fixed receiver can be successively insonified by all the pings transmitted along the survey line – their relative influence being defined by propagation losses rather than by angle selectivity.

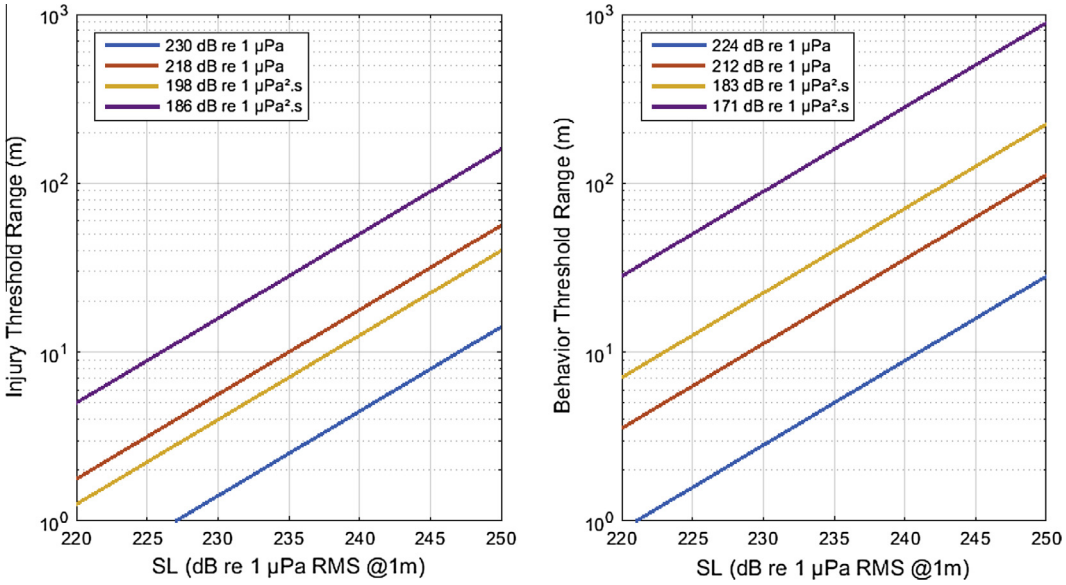

Fig. 12. Threshold ranges computed for MBES #3 along a survey line, for injury (left) and behaviour (right), as a function of the source level in a single-pulse configuration.

Table 2
Characteristic transmission parameters of three «generic» MBES. The characteristics listed here are typical of currently-met classes of systems. They do not strictly correspond to any commercially-available system.

	MBES #1	MBES #2	MBES #3
Nominal freq. (kHz)	100	30	12
Element beamwidth (°)	120	100	100
Along-track aperture (°)	1.5	0.5	1
Sector number (along; across)	(1; 1)	(3; 1)	(1; 7)
Along track Tx sector tilt (°)	0	−2°; 0°; 2°	0
Across-track sector tilt angle (°)	0°	0°	−55°; −30°; −14°; 0°; 14°; 30°; 55°
Across-track sector beamwidth (°)	120° (element)	100° (element)	28°, 18.5°, 16.5°, 16°, 16.5°, 18.5°, 28°
Pulse duration (ms)	1 ms	5 ms/ all sectors	10 ms/all sectors
Pulse number per ping sequence	1	3	7
Source level (dB re 1 µPa at 1 m)	220	235	240
Far-field conventional limit (m)	17	520	325
Typical absorption coeff. (dB/km)	36	6.4	1.2
Typical water depth (m)	200	2000	5000

Table 3
Values of SEL and SPL corresponding to threshold levels of acoustic signals received by marine mammals, according to injury and behavioural impact criteria [10].

	Injury criteria SPL (dB re 1 µPa)	Injury criteria SEL (dB re 1 µPa^2 s)	Behaviour criteria SPL (dB re 1 µPa)	Behaviour criteria SEL (dB re 1 µPa^2 s)
Cetaceans (low-, mid- and high-frequency)	230	198	224	183
Pinnipeds (in water)	218	186	212	171

4.3.1. Maximal received level

Regarding the maximal *SPL* received from a survey line, no difference has to be made with the previous case of a single ping. The ping corresponding to the minimal propagation loss has to be considered, which is normally the one corresponding to the closest point of approach (CPA) – although in case of a narrow Tx-sector the few pings received during the receiver's exposure to the main lobe should not present significantly different levels. So basically formula (16) remains applicable, taking the minimum value of $TL(R)$ over the survey line, i.e. for $R = R_{CPA} = Y$ (where Y is the orthogonal distance from the receiver to the line)

$$SPL = SL_{ML} - 20\log Y - \alpha Y + D_E(\psi_{CPA}) \tag{21}$$

where $D_E(\psi_{CPA})$ is the element directivity pattern value at the CPA. The radiation from the sidelobes, much lower, does not have to be considered here.

4.3.2. Sound Exposure Level

Consider now the SEL accumulated along the survey line, restricted first to the transmission by the main lobe, illustrated in Fig. 14. A given receiver point, located at an orthogonal distance Y from the line, will be exposed to a number of pings N_p given by the ratio between the beam aperture ($Y\Delta\theta$) upon reception and the step distance Δx between the successive pings on the survey line:

$$N_P(Y) = Y\frac{\Delta\theta}{\Delta x} = Y\frac{\Delta\theta}{VT_R} \tag{22}$$

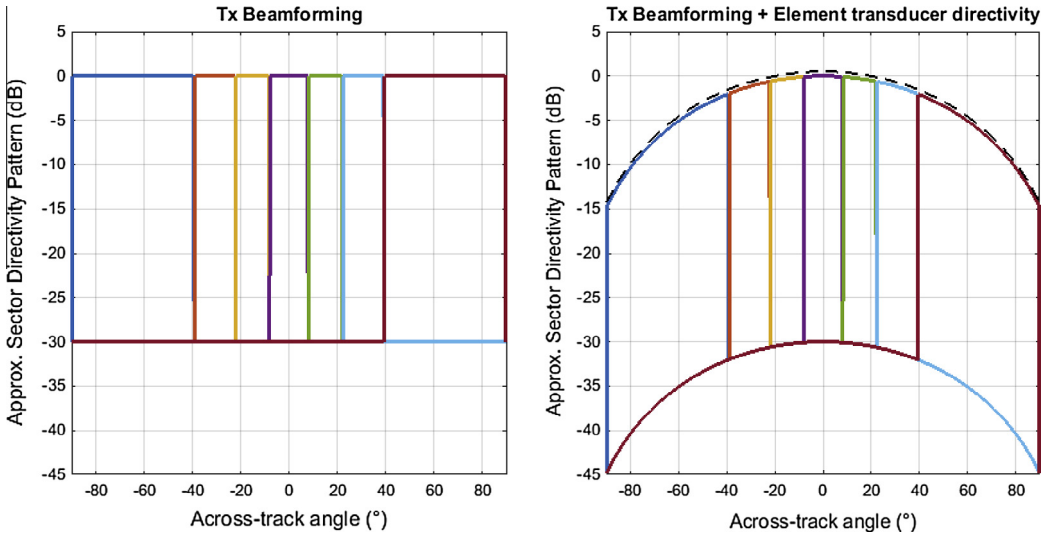

Fig. 13. Sound level radiated at 1 m by a multisector MBES, as a function of the transverse angle θ. Simplified directivity pattern for Tx-sector beamforming (left) and combined with element transducer directivity (right); to be compared with Fig. 7.

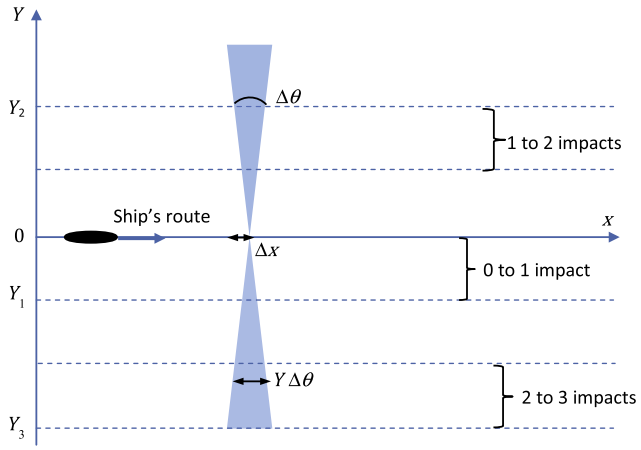

Fig. 14. Insonification by the main lobe of a MBES directivity pattern, plotted in a (x, Y) space (see text for definitions). The number of possible successive receptions on a fixed receiver increases with the range Y between the survey line and the receiver, depending the beam aperture $\Delta\theta$, and to the distance Δx run between two transmissions.

where V is the platform speed (in m/s) and T_R the pulse repetition delay (in s). By definition, N_p should be an integer number. However, in order to get a smoothed average of the cumulative SEL over the propagation medium, N_P is allowed to be non-integer. Also, in order to account for multi-swath transmission increasing the potential exposure at a given point, the number N_{SW} of transmitted swaths has to be applied to the number of received pings, so that finally:

$$N_P(Y) = N_{SW} Y \frac{\Delta\theta}{\Delta x} = N_{SW} Y \frac{\Delta\theta}{V T_R} \tag{23}$$

Hence the cumulative main-lobe SEL can be written as (20) expressed at $R = Y$ and increased by the number of received pings N_P given by (23), hence developed as:

$$SEL_{ML}(Y) = SL_{ML} + 10\log\left(N_{SW}\frac{\Delta\theta}{YV}\frac{T_P}{T_R}\right) - \alpha Y + D_E(\psi_{CPA}) \tag{24}$$

This approximated model is valid along the survey line provided that the nominal number of cumulative pings N_P has been reached. Hence it is not accurate at both ends of the line, where N_P decreases down to one half of its nominal value. It features explicitly the duty cycle T_P/T_R of the source (the relative amount of time during which the source is transmitting).

It is interesting to note that the averaged SEL accumulated along the line can be smaller than the SEL received from one ping. This apparent paradox is linked to the statistical nature of the model; at short ranges, the probability of insonification by the main lobe is smaller than unity.

Making equal the SEL values expressed from Eqs. (20) and (24), or equivalently searching for the number of effective pings $N_P(Y)$ to be equal to unity in Eq. (23), the limit range is readily found to be:

$$Y_1 = \frac{VT_R}{\Delta\theta N_{SW}} \tag{25}$$

With $V = 4$ m/s, $T_R = 10$ s, $\Delta\theta = 1°$ and $N_{SW} = 1$, the limit resulting range Y_1 is 2291 m.

Neglecting, in the first stage, the effect of elementary transducer directivity, the sidelobe transmission can be approximated by a spherical radiation, and the cumulative level along a survey line can be computed analytically (with a theoretical solution completed heuristically by addition of the directivity and absorption effects; see Appendix B), the SEL accumulated along a survey line and due to sidelobes from the N_S sectors can then be modelled as:

$$SEL_{SL}(Y) \approx SL_{SL} + 10\log\left(\frac{\pi}{2YV}\frac{T_P}{T_R}N_S\right) - \alpha Y + D_E(\psi_{CPA}) \tag{26}$$

This expression predicts a cylindrical-propagation loss (in $1/Y$ instead of $1/Y^2$). As for the main-lobe expression, it accounts for the duty cycle T_P/T_R of the source.

It is then readily possible to express the difference between the two contributions (from main lobe and sidelobes) to the cumulative SEL:

$$\Delta SEL = SEL_{ML} - SEL_{SL} = B + 10\log\left(\frac{2\Delta\theta}{\pi}\right) \tag{27}$$

which is interestingly independent of range, and depends only on the sidelobe relative level B and the main lobe aperture $\Delta\theta$. For a typical aperture of 1°, the corrective term $10\log(2\Delta\theta/\pi)$ is about −20 dB; hence the SEL difference, for a sidelobe level at −30 dB down from the main lobe, is only $\Delta SEL = +10$ dB, meaning the sidelobe contribution can hardly be neglected in the total SEL. Moreover, if the sidelobe SEL is increased by the number of

transmitting sectors, then the difference decreases: with a set of 10 sectors increasing SEL_{SL} by 10 dB, the sidelobe contribution to SEL equals the main lobe.

4.3.3. Total radiated field

The total SEL_T is obtained by adding the two contributions (from the main lobe and sidelobes, derived in Section 4.3.2) expressed in intensity natural values; coming back to the dB notation:

$$SEL_T(Y) \approx SL_{ML} + 10\log\left(\frac{T_P}{VT_R}\left(N_{Sw}\Delta\theta + \frac{\pi}{2}B_{nat}N_S\right)\right) - 10\log Y - \alpha Y + D_E(\psi_{CPA}) \quad (28)$$

where B_{nat} is the natural value of the level difference B between sidelobes and main lobe, given by $B_{nat} = 10^{-B/10}$.

4.4. Validation

In order to validate the approximate model presented here, the cumulative SEL is computed under two methods for comparison:

- A numerical summation of all the contributions from a discrete series of transmissions along the survey line;
- A direct application of the approximate formula (28).

The configuration features the MBES#3 (see Table 1) radiating along a survey line at a speed of 8 knots and a ping rate delay of 10 s.

The SEL field is computed in a horizontal plane located at depth 500 m. The computation is done successively for the main lobe, the sidelobes, and their combination. For each contribution, the results displayed in Fig. 15 (upper) feature a numerical simulation of all pings accumulated and plotted on the horizontal plane; then the average is computed along x, aimed at smoothing out the discontinuities due to the integer character of the number of locally-active main lobes of the Tx sectors. These smoothed results are plotted in Fig. 15 (lower) together with the 2-D plots, and with the results from the model formulas.

The main lobe contribution shows a striped structure of the field computed around the survey line axis, due to the discontinuous insonification at short ranges by the narrow Tx lobe. Conversely, the sidelobe contribution is very smooth, due to the high number of pings effective at a given point, and their stability along the line. On the average, the contributions of main lobe and sidelobes show the same magnitude. The approximated results provided by Eq. (26) (red lines on the lower plots) are in good agreement with the numerical computations. The greatest difference is observed for the sidelobe result at large y values; this is due to the approximation done in the TL and DF applied to the sidelobe contributions coming from wide horizontal angles (for which the approximation of the CPA range and angle are of lesser quality). This case is the main point of discussion: the fundamental model (spherical source, no absorption) presented in Appendix B, is derived without hazardous hypothesis – only the final application of directivity and absorption effects at CPA are stronger approximations. It should be noted that they tend to slightly overestimate the SEL, a trend which is desirable for case studies of impact assessment on MMs.

After validation of the analytical model, case studies can be readily addressed, limiting the computations to field estimations

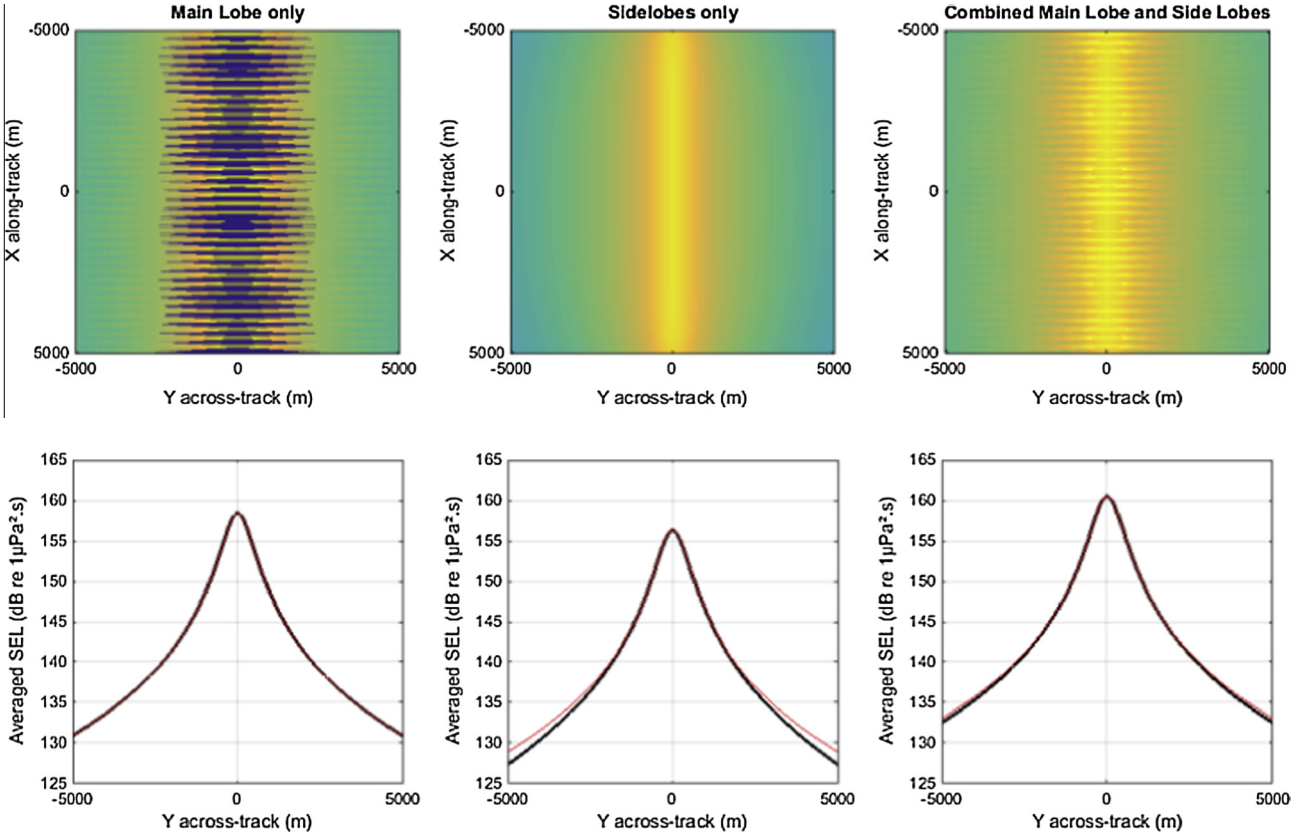

Fig. 15. Sound Exposure Level (in dB re 1 µPa^2 s) radiated by a MBES in the horizontal plane along a survey line. The three upper plots depict the SEL field obtained numerically (at a 500-m depth) by a discrete summation of all the ping contributions received in all points one the (x, y) plane, for respectively (from left to right) the main lobe, the sidelobes, and their combination. The lower plots present the SEL field across-track, averaged along the survey line, either numerically (black) or using the approximations (24–26) (red). (For interpretation of the references to color in this figure legend, the reader is referred to the web version of this article.)

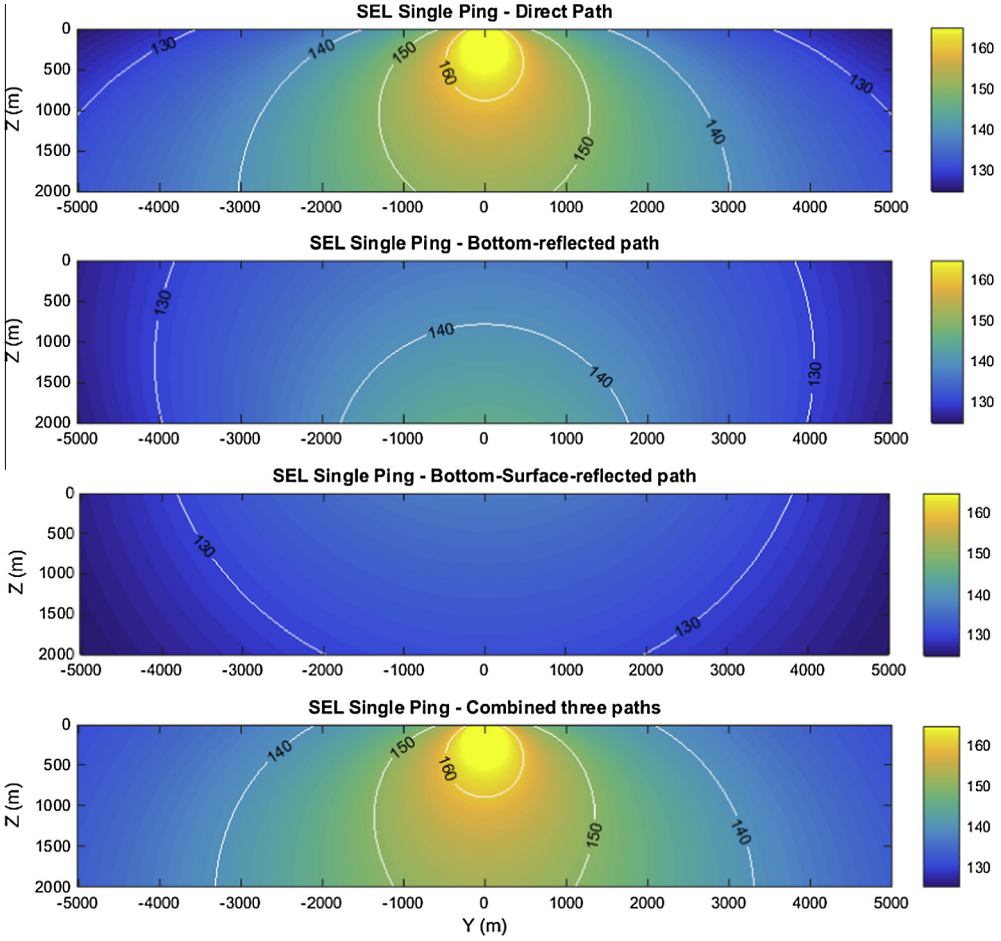

Fig. 16. Contribution of the first-order reflected paths to the SEL (in dB re 1 μPa^2 s), for a 12-kHz MBES and a 6-dB bottom-reflection loss: direct path (upper); bottom-reflected path (second); bottom-surface reflected path (third); and summation of the three contributions (lower).

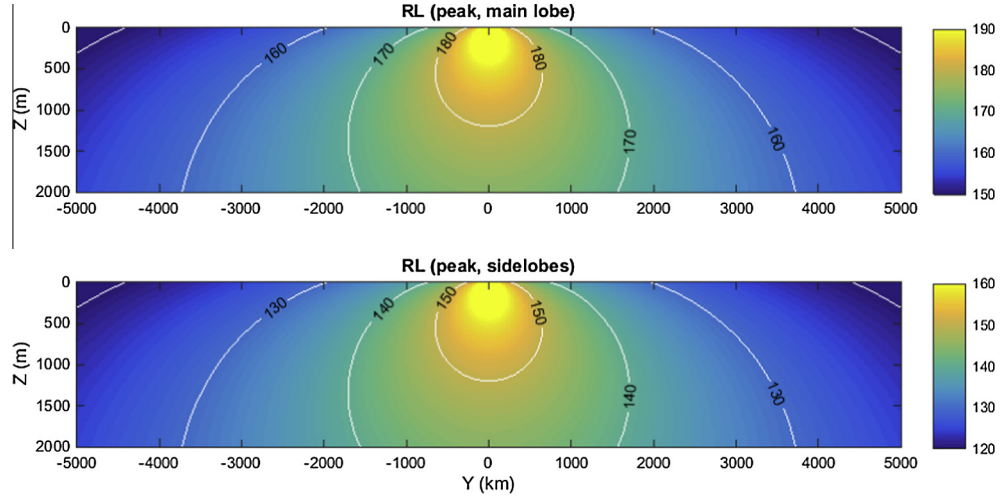

Fig. 17. Peak value of the Sound Pressure Level (in dB re 1 μPa) computed in the vertical plane for MBES #3, for the main lobe (upper) and the sidelobes (lower).

in the vertical plane, the field structure along the survey line in the horizontal plane presenting no real interest. Examples are presented in the following paragraphs.

4.5. Improved propagation model with first-order reflections

The relevance and accuracy of the propagation model can be much improved by accounting for the first-order reflected paths on the seafloor and sea-surface. A good approximation is to complete the direct path by the bottom-reflected (*B*) and the bottom-surface-reflected path (*BS*). On the one hand these contributions will "fill the gap" of the direct-radiated field close to the surface; on the other hand the higher-order reflections will usually lead to negligible contributions: for e.g. second-order reflected paths, the propagation path lengths are typically twice the first-order ones (hence on the average an extra-loss of 6 dB for

geometrical divergence, plus the absorption effect) as well as one more bottom reflection loss.

Fig. 16 illustrates the relative influence of the first-order reflected path; it presents the contributions on the one-ping SEL from (*D*), (*B*) and (*BS*) paths, and their summation. The case study is for MBES #3, considering a bottom-reflection loss of −6 dB. The plots make clear that, in this particular case, the reflected-path contributions contribute little to the resulting SEL field, although the conditions correspond to a rather reflective seafloor.

Despite the interest of the topic, we will not investigate here in more details the multipath structure impact on the MBES-radiated field; the purpose of this paper is rather to demonstrate the structure and magnitude of the radiated field, and to propose simple evaluation tools.

5. Application to a case study

5.1. Configurations

The case studied here features again MBES #3 presented in Table 2. This low-frequency system (12 kHz) provides a high Tx level (240 dB RMS or 243 dB Peak re 1 μPa at 1 m), and a transmission along seven across-ship sectors. Together with a low value of absorption coefficient (1.2 dB/km) this is the worst-case scenario, with respect to MMs impact, among the various possible MBES systems.

The radiation pattern is taken in its simplified form presented in the previous section – hence the transmitted level is not considered to be modulated by the directivity of the beamformed Tx sectors, but by the element directivity function.

The water depth is taken equal to 2000 m, and the pulse repetition rate is correspondingly 10 s. The propagation model is restricted to a simple direct-path transmission without accounting for interface-reflections – since it was shown previously that in this particular case the reflected-path influence is negligible.

The radiated field in SPL and SEL will be presented both for a single ping and, more interestingly, accumulated along a survey line. The purpose is to compare the values obtained from the modelling to the thresholds proposed in [10]. In this respect, the threshold values considered here are (Table 3):

- For maximal SPL: 230 dB re 1 μPa for pulsed sounds and for the three classes of cetaceans.
- For SEL: 198 dB re 1 μPa^2 s (for physiological effects) and 183 dB re 1 μPa^2 s (for behavioural disturbances) for pulsed sounds and for the three classes of cetaceans.

5.2. Field computation results

5.2.1. SPL estimation

The SPL computation is straightforward, both for the main lobe and for sidelobes. It is plotted in Fig. 17 together with iso-level curves in 10-dB steps.

The SPL values obtained for the main lobe are around 180 dB re 1 μPa at a range of typically 1000 m. Hence the injury threshold (230 dB re 1 μPa) cannot be met but at very short ranges from the sonar source. Using Eq. (1) gives, at the vertical (*DF* = 0 dB) a transmission loss of 13 dB, or equivalently a range of 4.5 m.

The SPL values in the sidelobe region are still 30 dB lower, and are negligible from an acoustic impact perspective.

5.2.2. SEL estimation – single ping

The SEL is computed here for one single ping, considering successively the main lobe (readily obtained from the SPL and the exposure duration) and sidelobes contributions (accounting for the number of sectors). It is plotted here (Fig. 18) together with iso-level curves at 10-dB steps.

These SEL values can be compared with the impact thresholds (198 and 183 dB re 1 μPa^2 s for respectively physiological and behavioural impact). It is clear from Fig. 18 that such thresholds cannot be met but at very short ranges from the source. The corresponding ranges inside the main lobe at the vertical are 13 m and 71 m. In the sidelobe region (21.5 dB lower) the potential impact is negligible.

5.2.3. SEL estimation – survey line

The SEL is cumulated along a survey line, for the main lobe, sidelobes, and combination of both. It is plotted here (Fig. 19) together with iso-level curves at 10-dB steps.

The computation results show that the SEL is dominated by the main-lobe effect – although the sidelobe contribution is only slightly lower. Interestingly the level of the average cumulative SEL is, at short ranges, lower than the SEL associated to one single ping. This effect, due to the statistical nature of the analytical model (at short ranges the insonification rate may be smaller than one effective ping) has been discussed previously.

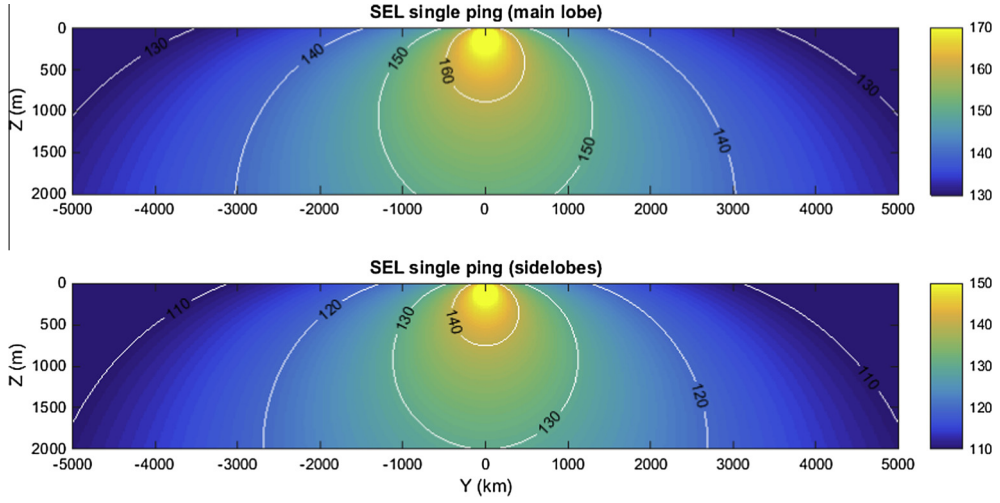

Fig. 18. Sound Exposure Level (in dB re 1 μPa^2 s) for one single ping of duration 10 ms, computed in the vertical plane for MBES #3, for the main lobe (upper) and the sidelobes (lower).

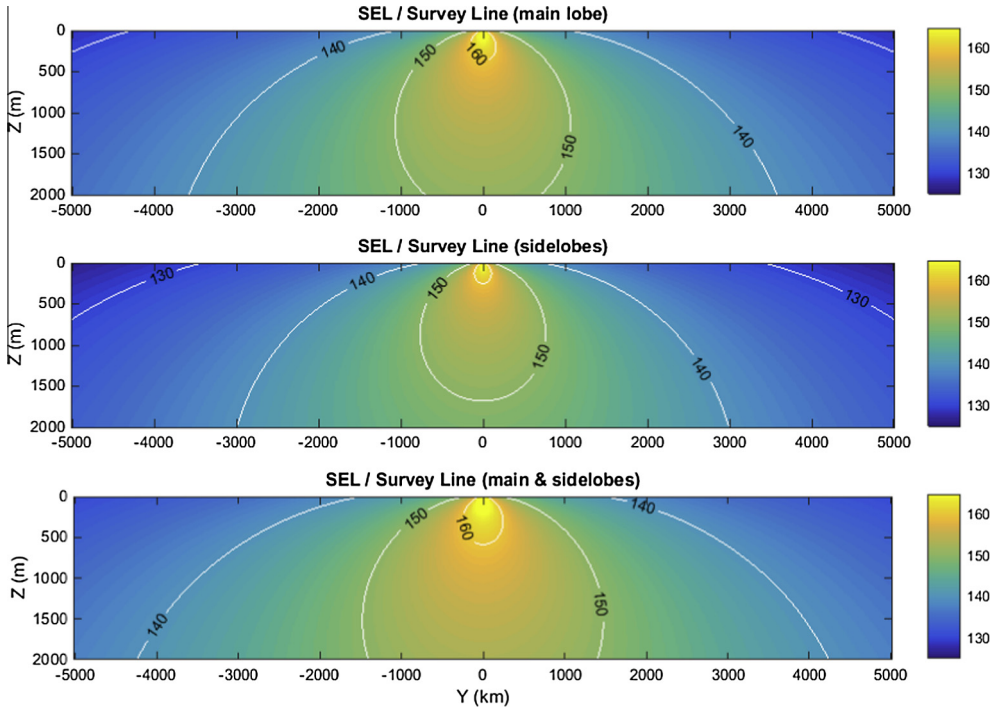

Fig. 19. Sound Exposure Level (in dB re 1 μPa^2 s) for a survey line at speed 8 knots, computed in the vertical plane for MBES #3, with pings of duration 10 ms and repetition rate of 10 s, for the main lobe (upper), the sidelobes (middle) and combined (lower).

The main lobe SEL is little different from the "single ping" result; only a small number of pings are effective due to the narrow aperture of the Tx lobe. Conversely, the sidelobe contribution to SEL, cumulated all along the survey line, cannot be neglected, and may reach a magnitude order comparable to the main lobe. It is then necessary to combine both contributions. However, this cumulative SEL remains well below the 198/183-dB threshold values.

6. Conclusions

The modelling elements presented here make it possible to compute a prediction of the field radiated by current MBES systems. The field can be expressed either as the maximum SPL (the peak value of the received signal) or as the sound exposure level SEL (expressing the total acoustical energy integrated along time). Both criteria can be used for impact studies either under the point of view of physiological effects (physical trauma of the auditory system) or behavioural disturbance (modification of the animal current activities); impact threshold values, as a function of animal species, are given in the literature [10].

The directivity patterns of the Tx sectors are described by the directivity function of a main lobe, and a continuum of sidelobes, whose effective average level is discussed in Appendix A. These beamformed lobes are modulated by the directivity pattern of the individual transducer elements forming the Tx array. At a given receiving point, the maximum SPL is given directly from the radiated level. The SEL is obtained from a compensation of SPL by the transmit duration; its sidelobe component has to account for the number of Tx-sectors, since the contributions of the various sectors are cumulative.

A set of three generic MBES configurations has been used here, not indicative of actual commercial systems but synthesizing typical parameters of today's current systems. The values of SPL and SEL for individual transmitted signals have been computed and plotted, both in the vertical and horizontal plane.

In a second step a simplified model has been defined in order to compute the actual insonification along a survey line; an analytical model has been proposed (Appendix B) making it possible to estimate readily the cumulative SEL along a survey line, and in good agreement with a numerical simulation accumulating the pings radiated along the ship's route. For the analytical approach, the radiated field is split into contributions from the main lobe and sidelobes; without surprise, the results show that significant values of SPL can be obtained only in the main lobe; less intuitively, the contribution of sidelobes integrated over numerous pings can indeed contribute significantly to the total SEL.

In all cases, the predicted SPL and SEL values fall in a range that makes them of little concern – using the threshold levels commonly accepted today [10]. The conclusions are relative to the particular case study presented here, but there is little chance that significantly different conclusions would be obtained for other configurations, since the case defined here (12-kHz multi-sector MBES system with a high source level and long pulse duration) is a worst-case scenario with respect to MBES impact on MMs.

To extend these various results, a number of refinements could be addressed in the future:

- The relative influence and impact of the frequency spectrum components outside the signal's nominal bandwidth. The point may be raised that marine mammals can hear sonar signals with a nominal frequency outside their hearing range; while this is strictly true, the magnitude of these out-of-band components is normally very low.
- The impact of multipaths: the work above has mainly assumed sound propagation in a direct-path mode, although briefly investigating an improved model featuring first-order reflected paths. It is of course understood that in many cases things are more complicated, with the presence of a number of multiple paths – normally not changing significantly the instantaneous SPL, but certainly increasing the SEL. When the number of multipaths gets high, a guided propagation regime happens, with TL

significantly less than in direct-path mode; however this regime happens at large range/depth ratio – hence for distant receivers for which the acoustical impacts are of less concern.

- The effect of topography and propagation configuration: particular conditions, such as a strong bottom slope or a surface channel in the sound speed profile, can lead to a local concentration of transmitted intensity. This does not increase the risks of physiological impacts which, as discussed above, can only happen at very short ranges from the source, but can extend the range of auditory detection of the transmitted signals by the animals.
- The variation of absorption coefficient with depth: neglecting the dependence of the sound attenuation with depth underestimates the received level of signals for deep-located receivers, such as diving mammals.
- The influence of near-field radiation phenomenon: the hypothesis has been made here of a far-field radiation, hence overestimating the received levels at short range.

The same approaches as above could be applied to other types of echosounders (single-beam echosounders, sub-bottom profilers, acoustic Doppler profilers) – that are structurally simpler than the MBES addressed here and also expected to raise fewer issues in terms of possible impacts to marine life. It should also be emphasized that the radiation by echosounder systems is structurally very different from the medium- and low-frequency active naval sonars (featuring a wide-aperture transmission and long modulated pulses).

To conclude, it is very likely that in a huge majority of cases, the acoustical energy radiated by MBES has very little chance to cause physiological damages or even behaviour changes (with reference to the impact thresholds proposed today in the literature). However, it should also be stated that the type of analysis proposed here, conducted from a sonar engineering point of view, is aimed at predicting quantitatively the amount of acoustic energy perceived by the animals; it says nothing about the possible disturbances caused by the content of the signal, which may be considered as unpleasant, or threatening, from subjective criteria completely different from the purely energetic considerations developed here. Addressing this aspect of things requires specific scientific studies in which a well-controlled population of animals is monitored during the use of a given sonar system; a convincing example of such an approach can be found in [21].

The predictive computations presented here, although simplified, may be still too heavy for most MBES users having to deal with impact assessment of their at-sea activity; moreover, the variety of commercial systems operated today is not so large, meaning that the same predictions of radiated level are prone to be computed multiple times by various operators of identical systems. MBES sonar constructors could indeed help the community of users by conducting themselves this computational exercise for the various items of their product lines, and making public the results. This would save time and concern to their customers, while avoiding possible controversies arising from an insufficient level of technical information.

Acknowledgements

This work was conducted in the framework of the IFREMER internal R&D project "PJ0807 – Acoustique Sous-Marine". The publication of this work was suggested and encouraged by Pr. Larry Mayer (UNH/CCOM, Durham, NH), who brought many improvements to the manuscript. The measured directivity pattern of EM 300 transducer is published here by courtesy of Kongsberg Maritime, thanks to Berit Horvei. The author acknowledges the support of his IFREMER colleagues involved in our common activity in sonar performance modelling and measurements.

Appendix A

A.1. Average sidelobe level

The sidelobe level of a shaded array depends on the shading law details [20], and the quality of the array sensors. With the classical Dolph–Chebyshev used in many systems, the sidelobe level is fixed at a nominal value (typically −25 to −30 dB).

The sidelobe amplitude oscillates below their nominal maximum value. Since the interest is here in average energy considerations (for the evaluation of SEL), it is proposed that the effective value of the sidelobe levels is considered instead. Hence a RMS average (of the amplitudes in natural values) is taken over the angles of the sidelobe region, leading to an average level at approximately 3 dB below the nominal maximum. See the illustration in Fig. A.1 (upper) for a 64-sensor array shaded in Dolph–Chebyshev at −30 dB: the average level of sidelobes is around −33 dB.

It is also known that the ideal performance of array shading may not be reached practically, due to non-compensated imperfections in the response of elementary sensors: a random variation in the array sensor sensitivity causes a degradation of the sidelobe pattern. It is difficult to give an *a priori* estimate of the magnitude of this effect. We simply propose here (Fig. A.1 (lower)) one representative simulation case of such a variation and its impact on sidelobe level: assuming a response variation of the sensors of ±1 dB in amplitude and ±15° in phase, the impact on the sidelobe level is approximately an increase of 3 dB of their RMS average level. In this example, the resulting level is increased from

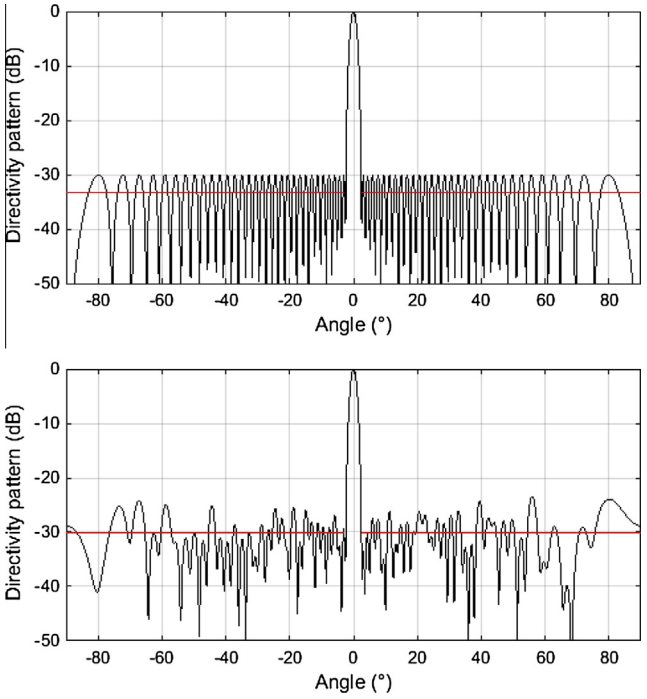

Fig. A.1. (Upper) Ideal directivity pattern of a linear array (64 sensors spaced at half a wavelength) weighted by a Dolph–Chebyshev law set at −30 dB for the sidelobe level. The angle-averaged intensity level over the sidelobe regions (red line) gives an average level of −33 dB. (Lower) Example of an actual directivity pattern in case of sensors with a randomized response (uniformly distributed within ±1 dB in amplitude, ±15° in phase). The angle-averaged intensity level over the sidelobe regions (red line) gives an average level of about −30 dB.

−33 dB to −30 dB, hence at the nominal value for sidelobe peak value.

So the magnitude of the beamforming performance degradation compensates approximately the gain (3 dB) associated to the angle-averaging. Consequently, in the following it will be considered that a nominal sidelobe rejection of –*A* dB will actually correspond to an average energy level of −*A* dB (compared to main-lobe regime) for the average intensity radiated in the sidelobe region.

Appendix B

B.1. A simple model for the field radiated by a source in motion along a survey line

We consider here the total insonification level by a point source in motion along a rectilinear trajectory, accumulated over time. The geometry is described in Fig. B.1.

The moving source radiates continuously with a maximum pressure level p_0 at 1 m, or an average squared pressure $p_0^2/2$. No source directivity is considered at this stage (hypothesis of a spherical source), so the field intensity received at a given point is only a function of the transmission loss for the oblique range $R = \overline{SM}$. A further approximation is that the absorption effect inside the seawater is negligible, and only the geometrical divergence is considered as a propagation loss effect. Making these assumptions, the received squared pressure at range R is given by:

$$p^2(R) = \frac{p_0^2}{2R^2} \tag{29}$$

The natural value of the SEL will be noted E_{SEL} in the following, with:

$$SEL = 10\log(E_{SEL}) = 10\log\left[\int p^2(t)dt\right] \tag{30}$$

The total intensity upon reception is given by the integral over time of the transmitted acoustic intensity affected by the propagation loss:

$$E_{SEL}(R_m) = \int_{-\infty}^{\infty} p^2(t)dt = \frac{p_0^2}{2}\int_{-\infty}^{\infty}\frac{dt}{R^2(t)} = \frac{p_0^2}{2}\int_{-\infty}^{\infty}\frac{dt}{R_m^2 + x^2(t)} = \frac{p_0^2}{2}\int_{-\infty}^{\infty}\frac{dt}{R_m^2 + V^2t^2} \tag{31}$$

where $R_m = \sqrt{y_M^2 + z_M^2}$ is the range at CPA (Closest Point of Approach) and V is the source speed. For simplicity, the reference time $t = 0$ is taken at the CPA instant. Finally an analytical solution to (31) can be obtained as:

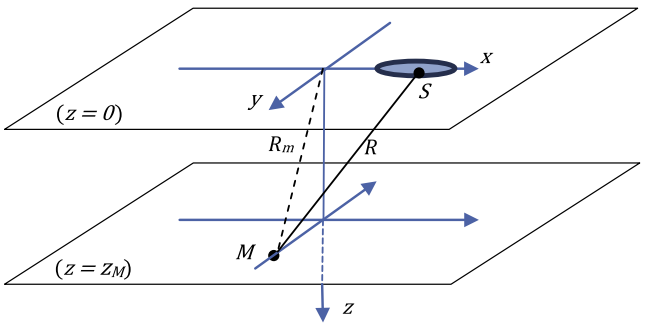

Fig. B.1. Geometry of the radiation from a source in motion along a survey line. The source is located in the plane ($z = 0$), and its trajectory is a straight line along the x axis. The receiving point M is located at coordinates ($x_M = 0$, y_M, z_M).

$$E_{SEL}(R_m) = \frac{\pi}{R_m V}\frac{p_0^2}{2} \tag{32}$$

This result corresponds to a continuous transmission from the source. Practically, the transmission is active only for a small fraction of time; hence the intensity upon reception is actually proportional to this duty cycle T_P/T_R (i.e. the ratio of the pulse duration T_P to the pulse repetition delay T_R); or, for an expression in dB, as $10\log(T_P/T_R)$. The cumulative squared pressure becomes:

$$E_{SEL}(R_m) = \frac{\pi}{R_m V}\frac{T_P}{T_R}\frac{p_0^2}{2} \tag{33}$$

Finally, the cumulative Sound Exposure Level, defined as the received acoustic intensity integrated along time, can be written as:

$$SEL(R_m) = 10\log\left[\frac{\pi}{R_m V}\frac{T_P}{T_R}\frac{p_0^2}{2}\right] \tag{34}$$

It is interesting to express SEL_{cum} directly from the source level $SL = 10\log(p_0^2/2)$:

$$SEL(R_m) = SL + 10\log\left[\frac{\pi}{R_m V}\frac{T_P}{T_R}\right] \tag{35}$$

Two main approximations have been done up to now. The source has been assumed to be spherical, hence without directivity pattern effect; and the absorption loss has been neglected. The directivity effect will be very grossly approximated from two aspects. First, the along-track directivity pattern tends to decrease the contributions from the extreme parts of the survey line; we will account for this effect by applying an arbitrary factor 1/2 in the result (32) of the SEL integration. Then the across-track directivity will be considered through its effect at the CPA point. Similarly, the absorption effect will be considered only through its effect on the TL at the CPA (since this range is obviously the main contributor). Without more detailed derivations or further justifications, these corrections are now integrated inside (35), which is now written as:

$$SEL(R_m) \approx SL + 10\log\left[\frac{\pi}{2R_m V}\frac{T_P}{T_R}\right] + DF_{CPA} + \alpha R_m \tag{36}$$

where DF_{CPA} is the source directivity function value at the receiver positioned at CPA, and α is the absorption coefficient in dB/m. This simple model will be useful in the following for expressing the SEL under a simple analytical expression and comparing it conveniently to the impact threshold values (if available). Compared with numerical simulations avoiding the various approximations done here, it also proves to be satisfactorily accurate. However it should be considered only as a convenient rough approximation.

References

[1] Lurton X. An introduction to underwater acoustics – principles and applications. 2nd ed. Berlin: Springer-Verlag; 2010.
[2] Lurton X, DeRuiter S. Sound radiation of seafloor-mapping echosounders in the water column, in relation to the risks posed to marine mammals. Int Hydrogr Rev 2011;6:7–18.
[3] Burkhardt E, Boebel O, Bornemann H, Ruholl C. Risk assessment of scientific sonars. Bioacoustics 2008;17(1–3):235–7.
[4] Southall BL, Rowles T, Gulland F, Baird RW, Jepson PD. Final report of the Independent Scientific Review Panel investigating potential contributing factors to a 2008 mass stranding of melon-headed whales (*Peponocephala electra*) in Antsohihy, Madagascar. Report to the U.S. Marine Mammal Commission; 2013. 75 pp.
[5] NOAA. Draft guidance for assessing the effects of anthropogenic sound on marine mammals; 2013. http://www.nmfs.noaa.gov/pr/acoustics/.
[6] Ellison WT, Southall BL, Clark CW, Frankel AS. A new context-based approach to assess marine mammal behavioral responses to anthropogenic sounds. Conserv Biol 2012;26:21–8. http://dx.doi.org/10.1111/j.1523-1739.2011.01803.x.

[7] Review of Naval Undersea Warfare Center (NUWC). Marine mammal acoustics exposure analysis model, 12–13 November 2008, Newport, Rhode Island; 2008. Available at http://www.nmfs.noaa.gov/pr/pdfs/permits/navy_acoustics_model.pdf.
[8] Houser DS. A method for modelling marine mammal movement and behavior for environmental impact assessment. IEEE J Ocean Eng 2006;31(76):81.
[9] NOAA; 2014. http://www.nmfs.noaa.gov/pr/permits/incidental/.
[10] Southall BL, Bowles AE, Ellison WT, Finneran JJ, Gentry RL, et al. Marine mammal noise exposure criteria: initial scientific recommendations. Aquat Mam 2007;33(4):411–522. http://dx.doi.org/10.1578/AM.33.4.2007.41.
[11] Urick RJ. Principles of underwater sound for engineers. New York: McGraw-Hill; 1983.
[12] Ainslie M. Principles of sonar performance modelling. Springer Praxis Books Geophysical Sciences; 2010.
[13] Ketten DR. Marine mammal auditory systems: a summary of audiometric and anatomical data and its implications for underwater acoustic impacts. NOAA Tech. Memor. NMFS, NOAA-TM-NMFS-SWFSC-256; 1998. 74 pp.
[14] Erbe C. Hearing abilities of baleen whales. Defense R&D Canada – Atlantic – contractor report #DRDC Atlantic CR 2002-065; 2002.
[15] Francois RE, Garrison GR. Sound absorption based on ocean measurements: Part II: Boric acid contribution and equation for total absorption. J Acoust Soc Am 1982;72(6):1879–90.
[16] Burdic WS. Underwater acoustic system analysis. Englewood Cliffs, NJ: Prentice Hall; 1984.
[17] Kongsberg-Simrad. Technical document related to the commissioning of EM 300 on R/V Le Suroit; 1999 [unpublished].
[18] Simrad. EM 12 hydrographic echo sounder – product description. Technical document Simrad P2302A; 1992 [unpublished].
[19] Hammerstad E. Sound levels from kongsberg multibeams. Kongsberg technical note; 2005. Available at http://www.km.kongsberg.com/ks/web/nokbg0397.nsf/AllWeb/DE3B0D5A997BE98EC1257B58004502AB/$file/EM_technical_note_web_SoundLevelsFromKongsbergMultibeams.pdf?OpenElement.
[20] Harris FJ. On the use of windows for harmonic analysis with the discrete Fourier transform. Proc IEEE 1978;66(1):51–83.
[21] McCarthy E, Moretti D, Thomas L, DiMarzio N, Morrissey R, et al. Changes in spatial and temporal distribution and vocal behavior of Blainville's beaked whales (*Mesoplodon densirostris*) during multiship exercises with mid-frequency sonar. Mar Mam Sci 2011;27:206–26.